5-2021

Flexible and Surface Modified ZnSnO3 Nanocubes for Enhanced Piezoelectric Power Generation and Wireless Sensory Application

Sk Md Ali Zaker Shawon
The University of Texas Rio Grande Valley

FLEXIBLE AND SURFACE MODIFIED $ZnSnO_3$ NANOCUBES FOR ENHANCED PIEZOELECTRIC POWER GENERATION AND WIRELESS SENSORY APPLICATION.

A Thesis

by

SK MD ALI ZAKER SHAWON

Submitted to the Graduate College of
The University of Texas Rio Grande Valley
In partial fulfillment of the requirements for the degree of

MASTER OF SCIENCE

May 2021

Major Subject: Chemistry

FLEXIBLE AND SURFACE MODIFIED $ZnSnO_3$ NANOCUBES FOR ENHANCED PIEZOELECTRIC POWER GENERATION AND WIRELESS SENSORY APPLICATION.

A Thesis
by
SK MD ALI ZAKER SHAWON

COMMITTEE MEMBERS

M Jasim Uddin, Ph.D.
Chair of the Committee

Narayan Bhat, Ph.D.
Committee Member

Tulay Atesin, Ph.D.
Committee Member

May 2021

ABSTRACT

Shawon, Sk Md Ali Zaker, Flexible and surface modified $ZnSnO_3$ nanocubes for enhanced piezoelectric power generation and wireless sensory application. Master of Science (MS), May 2021, 53 pp., 18 figures, 18 titles, 65 references.

Piezoelectric systems and their mechanisms are held in high regard, due to their cost-effective structure and mechanical proficiency to harvest renewable energy. In the present article, we propose an aluminum-doped zinc stannate ($ZnSnO_3$) piezoelectric nanogenerator that can be employed for the harvest of energy and sensory applications. In order to ensure and further enrich the piezoelectric mechanics and product outcome in our device, $ZnSnO_3$ was doped with 1 wt% to 5 wt% of aluminum nanoparticles. We reported that 2 wt% of aluminum-doped $ZnSnO_3$ showed the highest electrical output in terms of open circuit voltages and short circuit current.

The nanogenerator device achieved an average open-circuit voltage of 80 V to 175 V with a frequency range of 60 BPM to 240 BPM. This presented to be an unprecedented electrical output in comparison to period $ZnSnO_3$-based piezoelectric nanogenerators. With the presented high output-to-size ration taken into consideration, the device was installed into a helmet as an energy harvester and wireless human motion sensor which can harvest energy as well as can detect and transmit signals from mechanical human movement. Thus, transmuting a regular helmet into a smart helmet- indicates a promising future for the field of piezoelectric sensors.

DEDICATION

The completion of my master's studies would not have been possible without the love and support of my family. My mother MRS. NADIRA JAMIL, and my wife SURAYA YEASMIN, wholeheartedly inspired, motivated, and supported me by all means to accomplish this degree. Thank you for your love and patience.

ACKNOWLEDGEMENTS

I will be always grateful to my advisor Dr. M Jasim Uddin for his invaluable supervision in scientific research and for encouraging me with infinite patience and relentless positivity to complete my research. The endless love that I received from Dr. Uddin helped me to grow up both in my research and personal characteristics. I am thankful to my dissertation committee members: Dr. Atesin and Dr. Bhat for their insightful advice and constructive comments on my graduate research and thesis. I am thankful to Dr. Lozano for her guidance and help. I am also thankful to Dr. Padilla for her incessant help and support with the SEM, EDAX, and XPS characterization. I am thankful to Dr. Lin for her valuable guidance and suggestions on my manuscript. I would also like to thank our graduate coordinator Dr. Macossay and our office assistant Mr. Sanchez for making my time great in the graduate college of UTRGV. Much of this work would not have been possible without the help of my fellow lab mates: Valeria, Zaida, Sufian, Brishty, Musa, Farzana, Sadaf, Javier, and Ulises. I enjoyed discussing my research with them, especially Valeria, Zaida, and Sufian were directly supporting me with my experiment and manuscript. I would also like to thank my dormitory roommates: Omy, Ashif, and Arman for being so much helpful and cooperative all the time. Finally, but most importantly, I would like to thank my beloved parents for their unconditional love and my wife for her incessant support which kept me mentally sound during my graduate research.

TABLE OF CONTENTS

Page

LIST OF FIGURES

CHAPTER I

INTRODUCTION

In recent years, the insistence for renewable energy has heightened as a result of energy cataclysm from exhausting resources, global warming caused by the greenhouse effect, and air pollution as a result of fossil fuel fragmentation that increasingly declined the quality of human life. Therefore, there has been an ongoing surge for new and ingenious research, seeking innovative forms of renewable energy due to its environmental benefits and impeccable multiuse performance, such as sensors, portable electronics, wearable devices, and wireless transport systems [1-8]. Extensive studies and efforts have been applied to the contribution of harvesting clean energy [9]. Advanced designs such as, effective energy conversion and storage instruments that produce sustainable energy have become products held in high regard in the medical field, as some distinct designs have been proved to be reliable sensors used for health monitors. Among the diversity of energy conversion apparatuses, nanogenerators have a promising capability to convert low-frequency mechanical energies to electrical energy through devices such as triboelectric nanogenerators (TENG) and piezoelectric nanogenerators (PENG). Additionally, work by Pierre and Jacques Curie first depicted a mechanical stress-dependent surface charge generator Manbachi and Cobbold [10]. This brought to light piezoelectricity, the production of electric charge by exerting mechanical pressure. Piezoelectricity is created by linear electromechanical connections between electrical and mechanical states in a crystalline matter

that lack symmetry inversion. Piezoelectric materials have proved to be capable of producing a diversity of structural responses. Zhu et al. developed a piezo-photonic self-powered photodetector composed of a CdS NR array. The piezo-photonic effect can be used to regulate photodetection and pressure detection [11, 12].

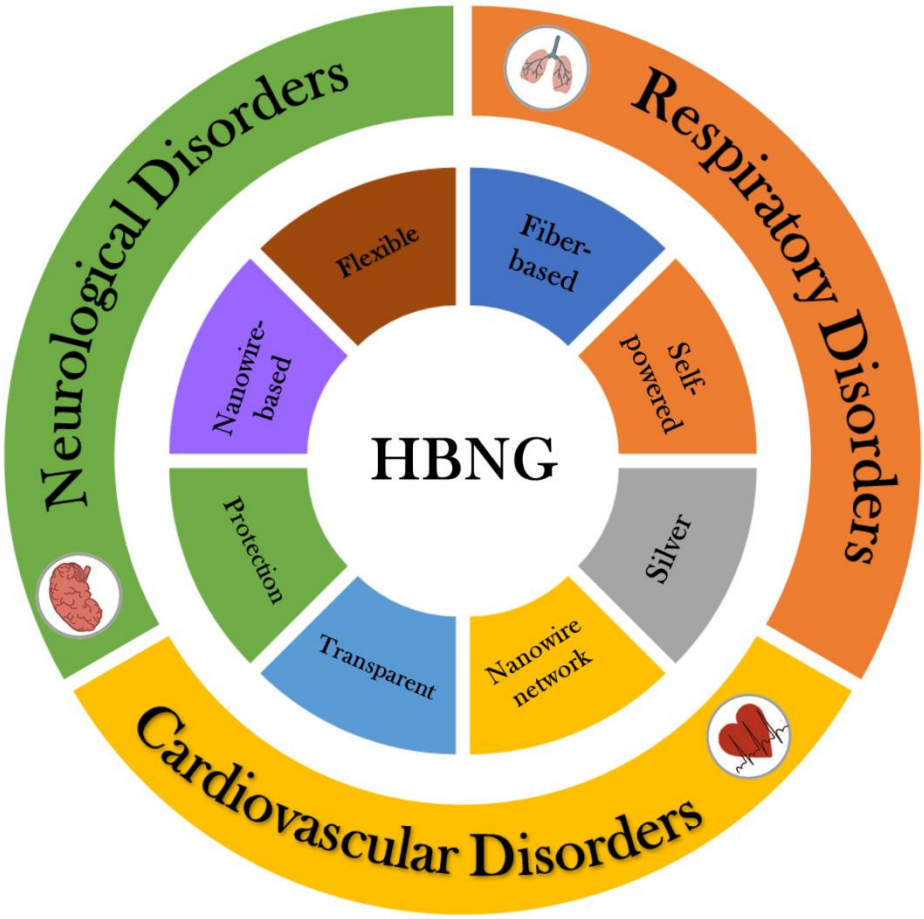

Figure 1: Schematic overview of Hybrid Nanogenerators classifications and various physiological disorders that can be monitored.

Combining the piezoelectric and triboelectric effect in a single device gives the concept of hybrid nanogenerators. Hybrid nanogenerators are also significant for their extensive use in the field of energy harvesting and health monitoring sensors. In figure 1, a schematic representation of several classifications of HBNGs can be found as well as different physiological disorders that can be monitored with these promising hybrid nanogenerator sensors comprising piezoelectric and triboelectric effects.

In concomitant with the au courant research on acquiring energy from innovative sources, has been accelerated, and motivated by increasing desire to address the energy crisis and demand for sustaining for wireless, portable electronic devices [9, 13, 14]. Widely available and abundant in the environment, ambient energy is one such source that has interested the scientific community [15]. Piezoelectric nanogenerators (PENGs), which can convert mechanical vibrations (e.g., biological movement, acoustic noise, low-frequency vibrations, airflow, etc.) into electrical energy are promising candidates for energy harvesting [16-19]. Additionally, they have many prospective applications such as in healthcare, self-powered sensing, wearable and implantable devices, etc. [16, 20-23].

The first PENG was fabricated using ZnO nanowires in 2006 [24], and since then, ZnO-based nanogenerators have continued to be researched and innovated due to their low cost, varied possible morphologies, and good piezoelectric properties. However, even as the output has been improved considerably over the years (from 9 mV to ~200V), it is still insufficient to fully realize powering of portable devices [25, 26]. Meanwhile, the potential of other materials in energy harvesting has been explored, including PZT which garnered attention for its high piezoelectric coefficient. However, its low conductivity as well as biocompatibility impedes its

output and limits its implantable or wearable applications, respectively; its lead component is also toxic [27].

Alternatively, Zinc stannate ($ZnSnO_3$), a multifunctional semiconductor, shows promise in the field of energy harvesting. Its high remnant polarization (P_r = 59 μC/cm^2) along the c-axis is conducive to higher output performance. Additionally, unlike many piezoelectric ceramics, which require electrical poling to align crystal orientations [25], $ZnSnO_3$ exhibits self-poling behavior under mechanical strain, facilitating easy nanogenerator fabrication [28, 29]. The carbon-thermal reaction, hydrothermal, coprecipitation, low-temperature ion exchange methods have all been used to create ZnSnO3 crystallites [28, 30]. However, since the material can present with various morphologies and structures and easily decomposes above 750 °C, the suitable synthesis method is vital to obtaining $ZnSnO_3$ with excellent energy-harvesting characteristics. Presently, $ZnSnO_3$ nanowires[31], microbelts [32, 33], nanorods [34], nanoplates [35], and nanocube [28, 36-38] have been used in energy harvesting. Among them, the nanocube morphology is one of the most common due to the low temperature solution method, which allows for particles with a smaller size and larger surface area [39]. Indeed, these characteristics are desirable for higher outputs in PENGs [28, 38].

However, one factor that limits the output of virtually all PENGs is the free carrier screening effect, by which free carriers diminish the piezopotential caused when a piezoelectric material is strained [32]. The suppression of these electrons would thus enhance the efficiency of a PENG and is a focus for many enhancement techniques. For example, the effects of doping, surface modifications, and particle treatment on the screening effect have all been investigated [40-42]. In terms of $ZnSnO_3$-based nanogenerators, Paria *et al.* recently added a CuO layer to their PENG, forming of a p–n heterojunction to screen for electrons [43]. Alternatively, other

techniques include the use of MWCNT to allow for a more uniform distribution of zinc stannate in PDMS[29] and micro-structuration to facilitate the distribution of force that can be converted into electrical energy [44]. However, doping, while investigated for other semiconductors including, has never been used for $ZnSnO_3$-based PENGs to enhance output through the suppression of the screening effect [45].

Herein, we present a novel technique to enhance the efficiency of a $ZnSnO_3$ at PDMS piezoelectric nanogenerator by doping zinc stannate with aluminum nanoparticles. $ZnSnO_3$ nanocubes were synthesized using the low temperature solution method, allowing for the deliberate formation of small particles sizes (average of 30 – 60 nm). This phenomenon of introducing $ZnSnO_3$ nanocubes of particle size range of 30 nm to 60 nm in nanogenerators is also unprecedented. Furthermore, Aluminum oxide (Al_2O_3) was added in varying amounts to accomplish Al nano particle doping into the ZnSnO3 structure. Experiment conducted using the range of 1% (w/w) to 5% (w/w) of Al nanoparticle doped in ZnSnO3 nanocubes, among which 2 wt% Al doped ZnSnO3 exhibited the highest piezoelectricity, and the doped $ZnSnO_3$ nanocubes was dispersed into PDMS to create the piezoelectric film. The device achieved an average open circuit voltage of 80 V to 175 V under a finger-tapping load frequency of 60 BPM to 240 BPM. The maximum short circuit current was found to be 20 µA with a power density range of 600 mw/m^2 to 2900 mw/m^2. Under finger tapping conditions, enough energy was produced to light 28 LEDs, showing the device's potential to convert ambient mechanical energy and power portable devices. Additionally, it has applications in self-powered sensing, such as when incorporated into a safety helmet to detect impact and motion. In this work we have also demonstrated the application of the as synthesized piezoelectric film by incorporating it into a safety helmet which was capable of detecting human motion while walking and running. A

circuit comprised of microprocessors also designed to show the wireless motion sensing capability of this Al doped $ZnSnO_3$ PENG.

CHAPTER II

BACKGROUND ON PIEZOELECTRIC NANOGENERATOR

Piezoelectricity potential in sensory applications is widely recognized by the scientific community. The main advantage of this technology is its ability in responding to pressure with an electrical output without an external power source. This characteristic allows for designs to be engineered with convenience and practicality in mind. Piezoelectricity sensory applications for human health monitoring has been steadily advanced by previous research, and several studies have created biomedical sensors centered on piezoelectric properties [46]. In 2018, Han et al. constructed a compact battery-free and wireless full-body sensor for temperature and pressure [47]. Using a spiral structure of thin, monocrystalline silicon membrane, a piezoresistive material, the researchers were able to integrate a pressure-sensing element into the sensor along with temperature sensing capabilities achieved through a thermometer detector in a near-field communication (NFC) chip [47]. Here, temperature sensor is the NFC microchip; the pressure sensor is made of silicon membrane and PDMS covers the sensor. The sensor could be charged, and data retrieved, wirelessly through radio waves from a phone or a similar device. Such sensor designs have immense applications in the human healthcare field as it offers 24-hour full-body monitoring that can be used to detect and prevent bedsores in bed-ridden patients. The structure and function of the sensors can be seen in the following Figure 2.

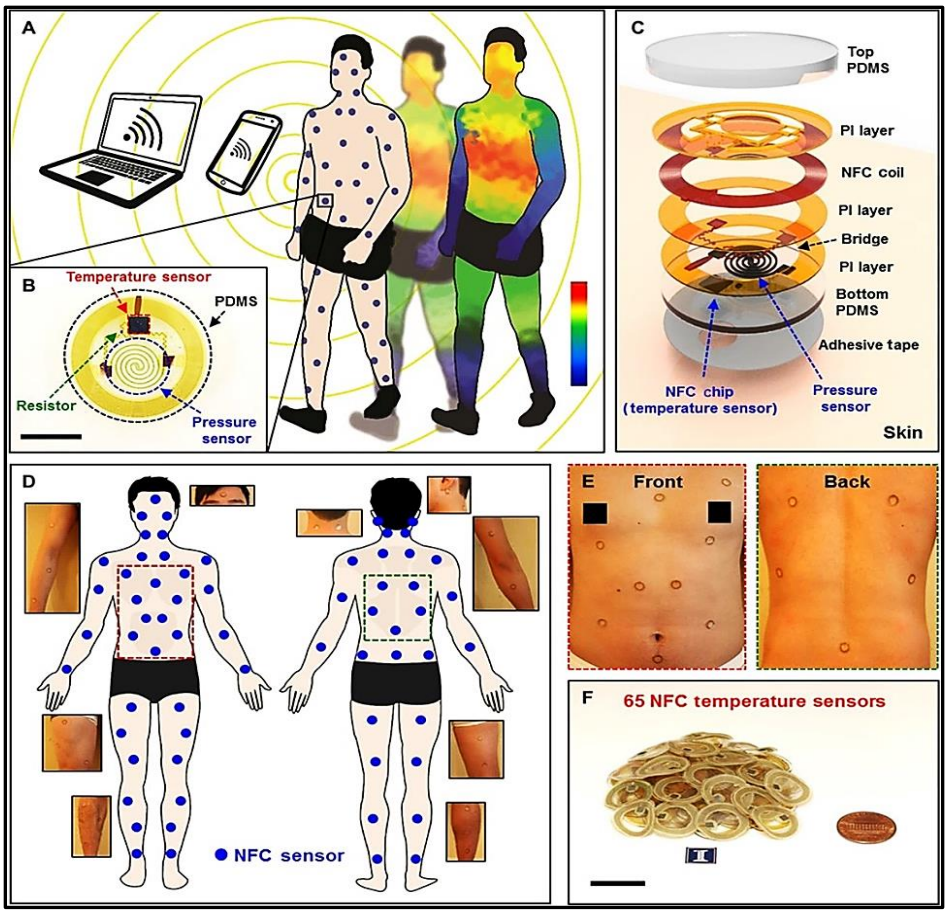

Figure 2: Overview of the wireless, battery-free sensors for full-body monitoring. (A) Illustration of the sensors applied for full-body monitoring and wirelessly transmitting information about temperature and pressure; and (B) top-view illustration of the sen sensor with 8mm scale bar; (C) schematic diagram showing the device structure; (D) illustration showing the distribution of 65 wireless sensors on the body and corresponding photographs; (E) images showing the distribution sensors on the front and back of the body, with red and green boxes; (F) images of 65 sensors with a penny for scale and a 16mm scale bar.

Another potential of PENG in health monitoring is in wearable fabrics. A fiber-based PENG is fabricated using zinc oxide nanowires and polyvinylidene fluoride around a conducting fiber [48]. Under ~ 0.1% strain, the device was able to reach a 32mV open-circuit output of voltage and a 2 $nAcm^{-2}$ closed-circuit current density. The fiber devices can also be superimposed by connecting them in series resulting in an open-circuit with higher output voltage (~85 mV) than either device individually (~40 mV and ~55mV). These results can be seen in Figure 3 (a-f).

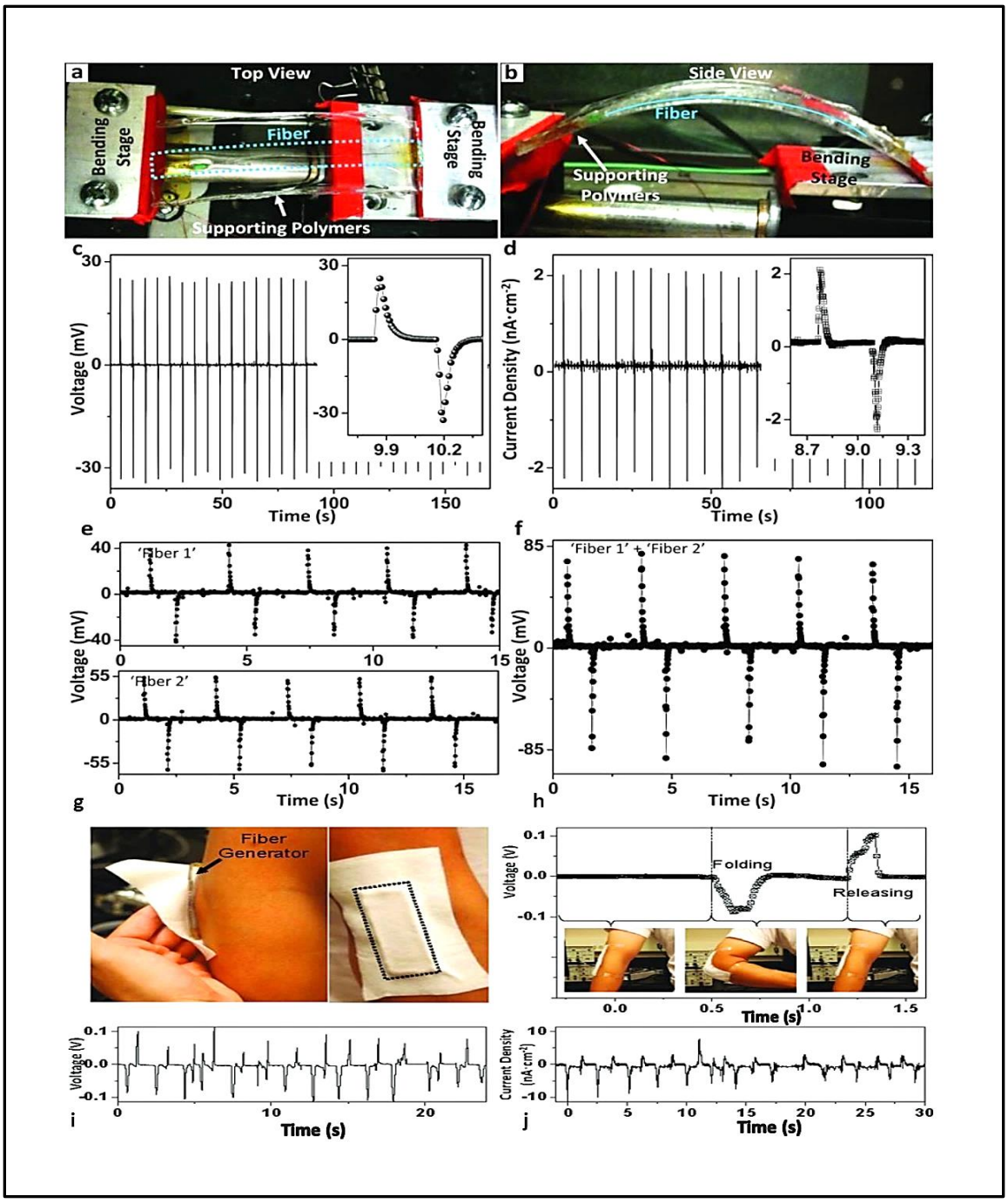

Figure 3: Photographs and electrical outputs of hybrid-fiber nanogenerators. Top-view (a) and side-view (b) of a hybrid-fiber device attached to a PS substrate and covered in PDMS for uniform stress, on a bending stage. Open-circuit output voltage (c) and close closed-circuit output current density of a fiber device (d) under a strain of ~ 0.1%. Open-circuit voltage outputs (e) of two

different fiber devices, labeled ‘Fiber 1’ and ‘Fiber 2’, under a strain of ~ 0.1%. Open-circuit voltage output of Fiber 1 and Fiber 2 (f) connected in series under a strain of ~ 0.1% and at a strain rate of ~ 2.3% s^{-1}. Photographs of the hybrid-fiber device (g), and PDMS/PS were attached in the same way and for the same reason as in (a). Open-circuit voltage output (h) of a fiber device from the flexion and extension (folding and releasing respectively) of the elbow. Open-circuit voltage (i) and closed-circuit current-density output (j) of a fiber device from several cycles of flexion and extension.

The device depicted in Figure 3 opens the opportunity for wearable nanogenerators that could monitor a patient’s motion and have applications in physical therapy where tracking the speed or strength of muscle movements is valuable. This application is further supported by the device’s output in response to movement when attached to the elbow, as shown in Figure 3 (g-j).

Additionally, in 2019, researchers were able to create a multifunctioning monitoring system by including a piezoelectric micromachined ultrasonic transducer (pMUT) array to detect relative humidity and room temperature [49]. The pMUT array was partially coated in polyethyleneimine (PEI)/graphene oxide (GO) and exhibited a high sensitivity of 748 Hz/%RH along with good linearity. The study demonstrates a way to utilize piezoelectricity to sense factors beyond pressure. Therefore, it is evident that piezoelectricity has a high potential versatility regarding its sensory capabilities.

Recent works demonstrated factors that promise the feasibility of piezoelectricity in widespread biomedical sensor applications. Interestingly, Onion Skin Based Piezoelectric Nano Generator (OSBPNG) could monitor the output sensitivity [50] of the throat movement during coughing (≈0.30 V), swallow pass (≈0.86 V), and drinking of water (≈0.20 V). In addition to this, the device could harvest green energy from throat voice signals by generating the sound of

“START” and “STOP” and it could also differentiate these two sounds in terms of electrical output. The high sensitivity of OSBPNG was further confirmed by harvesting energy from up-down neck movement and generating output signals in the range of ≈2.0 V to ≈3.5V from the falling of leaves from different height with various weights. These results strongly supported the onion skin based nanogenerator as a highly sensitive and potential energy harvester which can continuously produce output for longer cycles (up to 10000 cycles, 2000s), concluding it as a durable and mechanically stable alternate source of energy. All these applications are depicted through Figure 4.0 (a-i) [51] [52]. Additionally, in Figure 4.0 (j-k), prawn shell based nanogenerators are depicted that can produce electrical output upon throat movement and artery movement. Furthermore, prawn shell-based nanogenerators are also found to generate electricity from throat movement [53].

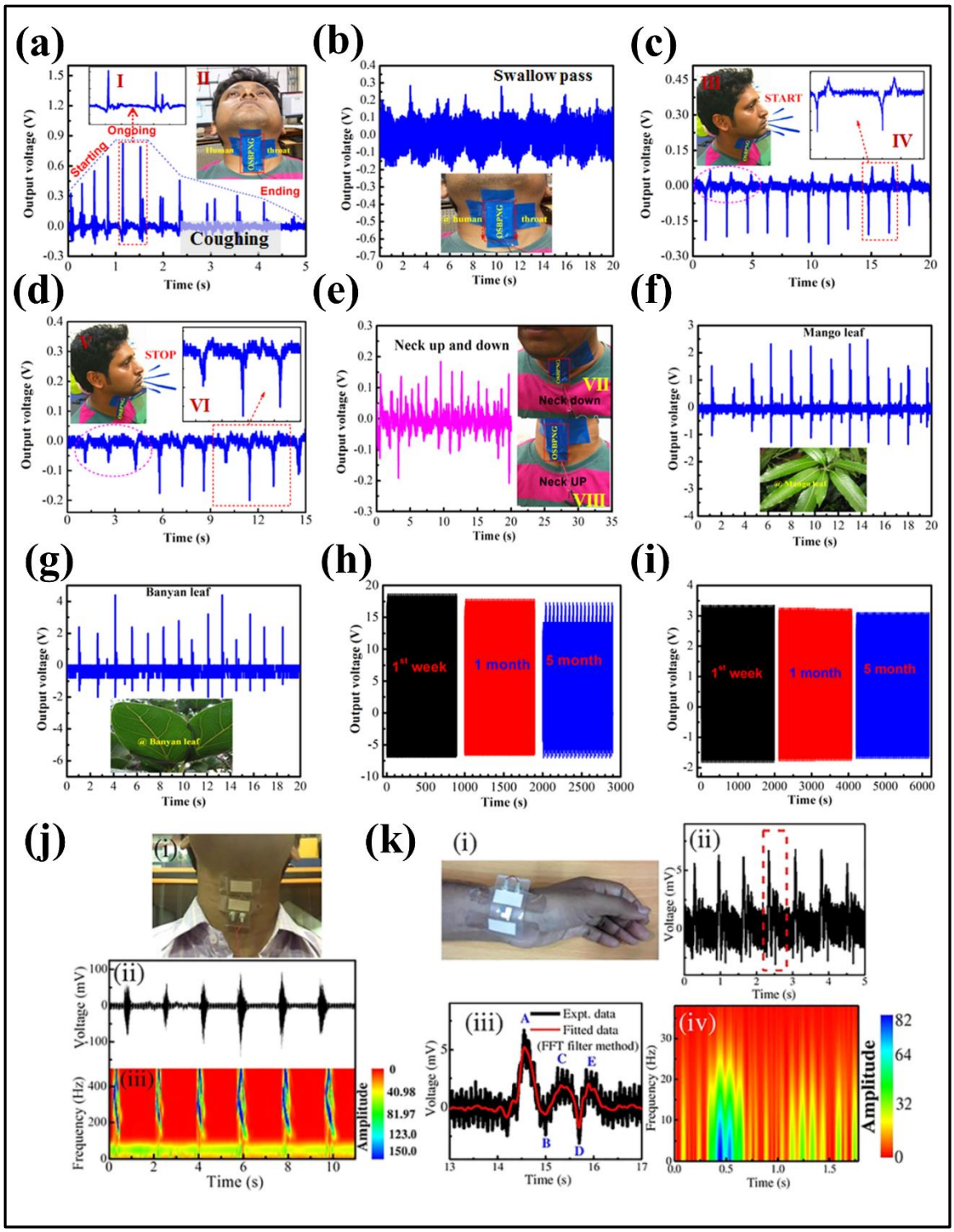

Figure 4: Output voltage of onion skin based nanogenerator attached to the throat when (a) coughing, (b) swallowing, (c) saying "start", (d) saying "stop", (e) nodding up and down. The

voltage output when a (f) mango leaf and (g) banyan leaf was dropped, showing the sensitivity of the generator. The stability of the nanogenerator when (h) hand punching and (i) sewing machine vibration. A prawn shell based nanogenerator attached to the throat (j-i) with its corresponding output values (j-ii). A prawn shell based nanogenerator attached to the wrist (k-i), with its corresponding outputs of (j-ii) wrist pulse vibration. The data was enlarged, and noise was removed (k-iii) and an STFT spectrogram was selected for a single pulse wave (k-iv).

Piezoelectric nanogenerators made of biodegradable materials offer several unique advantages. Firstly, biodegradability is important in reducing pollution. Secondly, cost-efficiency allows these sensors to be integrated into the healthcare system without huge financial barriers. Finally, the high sensitivity of these biodegradable piezoelectric sensors allows them to play a key role in monitoring the often-minute mechanical motions of the human body.

In recent years, detectors for certain chemical markers have been developed based on the piezoelectric effect. A self/powered breath analyzer based on PANI/PVDF Piezo-Gas-Sensing Arrays for diagnostics application was developed in 2018. The device works by converting energy from blowing of exhaled breath into electrical sensing signal without any external power sources. There five sensing units in a single device can be used for diagnosis of liver cirrhosis, airway inflammation, diabetes, and asthma. Another detector based on the piezoelectric effects, is a noninvasive electronic skin that couples the piezoelectric effect with a biosensing unit. The piezo-biosensing unit matrix is comprised of enzymes modified on the surface of ZnO nanowires. The electronic-skin can detect lactate, glucose, uric acid and urea in the perspiration through actively outputting piezoelectric signal (driven by body movement) [54-56]. These two sensors use the piezoelectric effect, and they couple it with other chemical detectors to identify body metabolites.

The innovation of flexible piezoelectric material increases the practicality of piezoelectricity as a human health monitor. Perovskite-structured ceramics, such as lead zirconate titanate (PZT), and lead magnesium niobate (PMN) show excellent piezoelectric properties. Although the toxicity of lead oxides in ceramics is debated, for biomedical applications, this concern has focused the research efforts on lead-free piezo materials, including polymers, ceramics, and composites, both in the form of film and fibers [57, 58]. Among them, a low-cost lead-free piezoceramic entitled with piezoelectric effects is barium titanate ($BaTiO_3$). Anyway, the use of $BaTiO_3$, PZT, and PMN-PT perovskite salts to construct piezoelectric thin films has allowed for greater mechanical-to-electrical conversion efficiency and thereby a more sensitive sensor [59]. PZT thin films were even used for detecting cellular deformations in the nanometer range. A key advantage of a flexible piezoelectric nanogenerator is its ability to conform to the irregular shapes of human skin and internal organs, being able to effectively monitor and harvest the mechanical motions of the human body. For example, a flexible piezoelectric material can be implanted on the surface of the heart, detecting the frequency and pressure of its beats while harvesting the energy to possibly maintain a pacemaker. Flexibility opens many opportunities for PENG to be used as a health sensor.

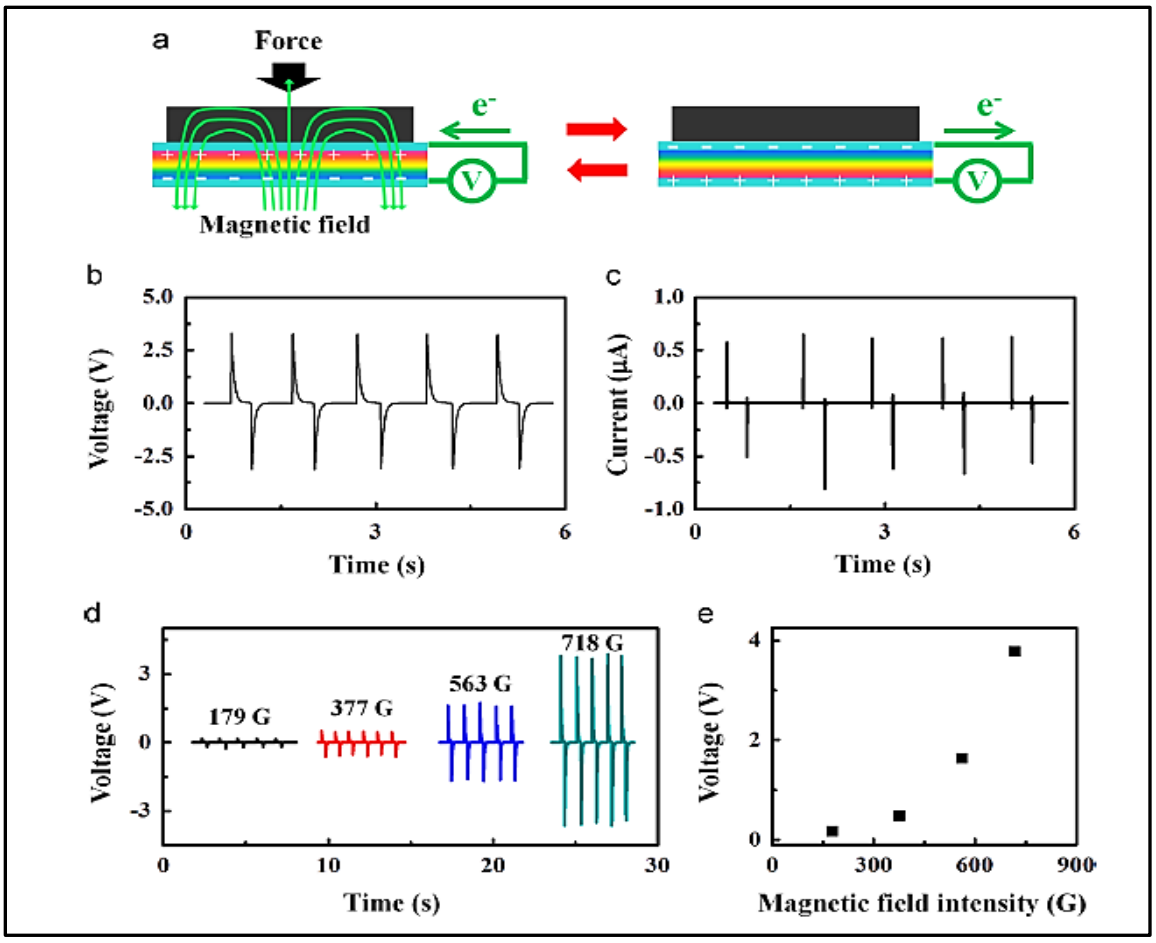

Figure 5: (a) Schematic diagram of WLNG and its working mechanism, (b) Output voltage of the WLNG, (c) Output current of the WLNG, (d) Voltage vs time plotted for different magnetic field intensities, and (e) peak output voltage plotted vs magnetic field intensities, and (e) peak output voltage plotted vs magnetic field intensity.

Another application for biomedical sensing is to use a piezoelectric generator as the power source of another sensor. Cheng and coworkers created a PENG using BZT-BCT nanowires that, instead of harvesting the body's mechanical energy, generates electricity through an external changing magnetic field [60]. Challenges to this design include the inconsistent mechanical motion of the human body which makes it difficult for PENG to power another device without a storage battery. The design presents a significant approach integrating

piezoelectricity into a sensor system to eliminate the need for wires or batteries. More information about the working mechanism of the device can been seen in Figure 5.0 (a). Under a changing magnetic field created by an electromagnet, the current and voltage can reach 810 nA and 3.3 V respectively as shown in Figure 5.0 (b-c). Additionally, Figure 5.0 (d-e) shows voltage output under different values of magnetic field intensity, with an increase in field intensity exponentially affecting voltage. The output reaches a voltage of 3.9 V and a current of 1.17 μA.

CHAPTER III

METHODOLOGY

Synthesis of Zinc Stannate (ZnSO3) Nanocubes

All the chemicals were of analytical grade from Sigma Aldrich and used without further purification. The low-temperature solution method was used to synthesize the ZnSnO3 nanocubes [39]. 20 mmol of both ZnSO3 • 7H2O and Na2SnO3 • 3H2O were each dissolved in 100 ml DI water, making two solutions. The former was placed in an ice bath to maintain the temperature between 1 to 2 °C while the second solution was added dropwise. The 1:1 molar ratio mixture was allowed to react at a temperature of 1 to 2 °C for 12 hours, after which the solution was centrifuged (Fisher HealthCare© Horizon Model 614B) and washed with ethanol and DI water to remove any impurities. The centrifuged product was placed in a (Ney© Vulcan 3-1750) oven to dry for 12 hours at 110 °C. The experimental procedure concluded with ZnSnO3 nanocubes with an average particle size of 30-60 nm.

Doping of Aluminum in Zinc Stannate:

Aluminum oxide (Al_2O_3) mesoporous particles (3.5 nm) and the synthesized ZnSnO3 nanocubes were each dissolved in separate solutions, gradually mixed together and vigorously stirred for 3 hours. Afterward, the compound solution was centrifuged, washed with ethanol to remove impurities, and placed in an oven for 12 hours to dry at 120 °C. The newly dried powder was mortared and pestled for 1 hour to ensure uniformed mixing before being placed in the oven

for 8 hours at 600 °C for calcination. The calcined Al doped ZnSnO3 powder was washed thoroughly with DI water, then ethanol to remove any unwanted impurities.

Nanogenerator Fabrication:

To prepare the Aluminum-doped $ZnSnO_3$ piezoelectric film, Polydimethylsiloxane (PDMS), Ethyl acetate, and a curing agent were combined in a ratio of 10:6:1 and vigorously stirred. Subsequently, 20 wt% of the compounded Aluminum-doped ZnSnO3 powder was added to the PDMS solution and stirred for 3 hours to uniformly disperse it. The resulting solution was placed into a Petri dish, vacuumed for 1 hour to remove air pockets, and dried in an oven for 5 hours at 120 °C, forming the piezoelectric film. After being bilaterally attached to two pieces of copper tape and wire, the film and electrodes were enclosed (to enhance durability) with PDMS solution composed of PDMS, Ethyl acetate, and a curing agent in a 10:1:2 ratio. The encapsulated film was dried in an oven (Ney© Vulcan 3-1750) in 3 intervals: 1 hour at 60 °C, 1 hour at 100 °C, and 3 hours at 120 °C.

Electrical Characterization:

The device was attached bilaterally with two pieces of copper tape, which worked as the electrodes. Copper wires were used to connect the electrodes. Then the device was connected to the VersaSTAT3 machine to measure the piezoelectric output voltage and current. Results were confirmed by the measurement with Tektronix TDS 1001B oscilloscope while connecting the electrodes with the nanogenerator.

Morphological characterization:

Scanning Electron Microscopy (SEM) characterization, Energy Dispersive Spectroscopy (EDS) mapping, and EDAX compositional analysis of the Al doped ZnSnO3 piezoelectric material samples was performed using a JEOL 7800 F Field Emission Scanning Electron Microscope, equipped with an Electron Dispersive X-ray Spectroscopy system (EX-37270VUP).

XRD measurement:

XRD was performed on a BRUKER™ D8 advance X-ray diffractometer with Cu Kα1 radiation (λ = 1.5406 Å, 40 kV, 40 mA). The output data were collected in a scanning mode in the 2θ range from 10° to 90° with a scanning step size of 0.05° at a scan rate of 0.6° min^{-1}

CHAPTER IV

RESULTS AND DISCUSSION

It has been reported that optimized distribution of dopants parallel to the [0 0 1] direction in ABO3 type perovskite systems contribute to the enhanced piezoelectric potential of the perovskite system [61].

In our work, during the calcination of Al doped ZnSnO3 powder at 600 ˚C, Al^{3+} ion diffuses into the lattice parameter of ZnSnO3, thus causing a distortion of the ZnSnO3 structure.

The Al^{3+} substitution at A-site can increase the doping level of Sn4+ at the B-site, maximizing distortion upon mechanical stress. The ionic radius of Al^{3+} (0.62 A˚) is close to the ionic radius of Zn^{2+} (0.88 A˚) and Sn^{4+} (0.83 A˚). Thus, the larger mismatch of the A-site cation to the B-site cation plays a key role in decreasing the lattice parameters, and the resulting distortion of the crystal structure contributed to the Al doped ZnSnO3 structure. Thus, the Al doping in ZnSnO3 were capable of producing significantly higher electrical output without any kind of poling operation.

Moreover, with the unprecedented smaller cubic crystal size of ZnSnO3 (30nm-60nm) in a piezoelectric nanogenerator, it possesses a higher surface area and uniform distribution of mechanical stress induces greater distortion of lattice parameters which results in additional electrical output.

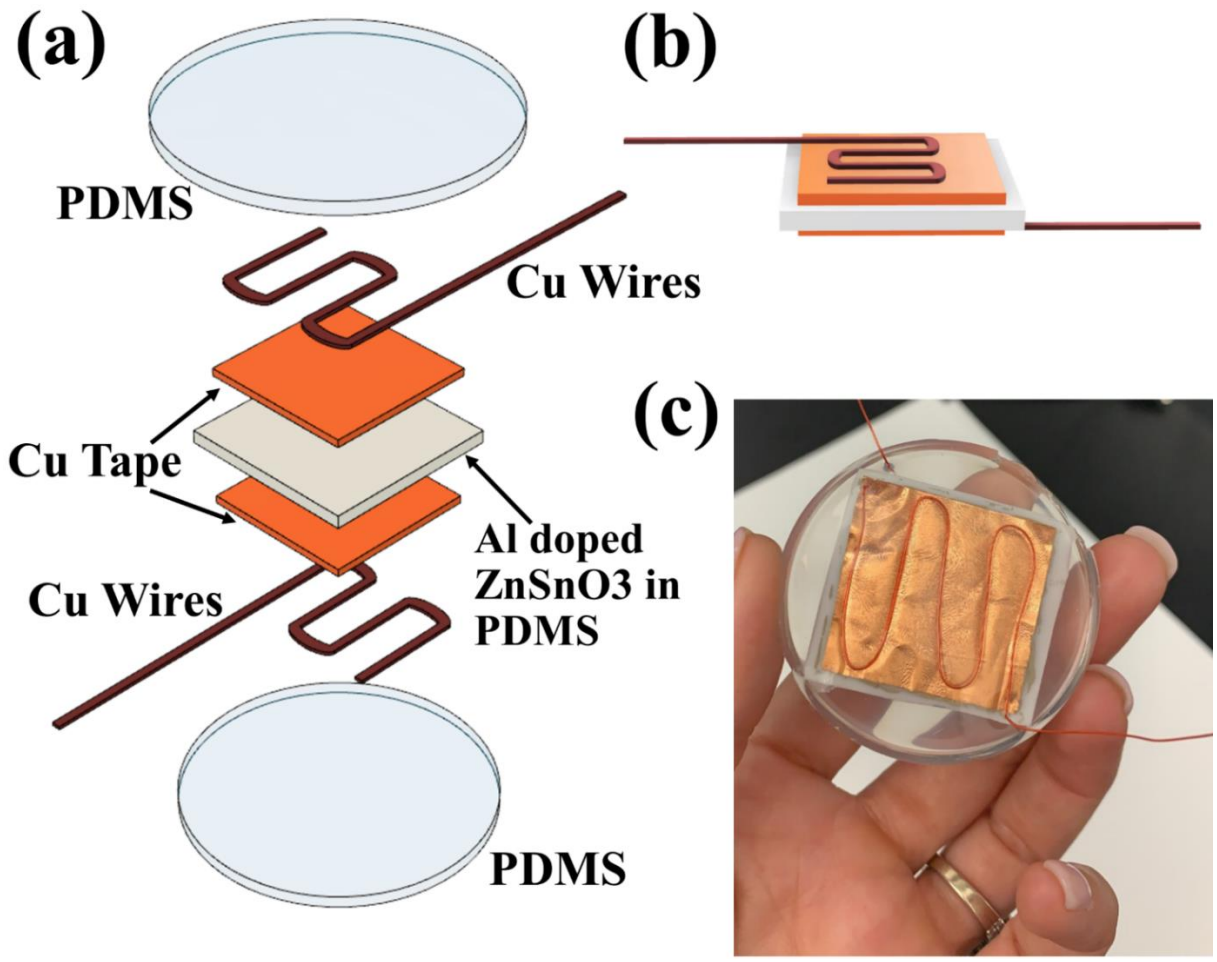

Figure 6: Detailed schematic view of the (a) encapsulated Al doped ZnSnO3 piezoelectric film and (b) the Al doped ZnSnO3 piezoelectric film with electrodes. (c) An image of the film in comparison to hand.

Figure 6, and Figure 7 illustrate the structure and working mechanism of the PENG. The as-fabricated Al-doped $ZnSnO_3$ – PDMS (Figure 6-a) film was sandwiched between two layers of thin copper tape attached to copper wires, which served as the electrodes to conduct the electrons from the film. Together, these pieces formed the functional component of the PENG as shown in Figure 6 (b). Next, the film and electrodes were encapsulated with PDMS to enhance

the device's durability against various environmental conditions and direct impacts. The device can be seen in Figure 6 (c) in comparison to the size of a hand.

The working mechanism of the device can be understood by first investigating the effect of mechanical load on the Al-doped $ZnSnO_3$ nanocubes. At first, the ions within each nanocube particle are about uniformly distributed. However, when an external force is applied, such as with the pressure from a finger, the compression of $ZnSnO_3$ structure creates a piezopotential from the polarization of its ions, as seen in Figure 7.

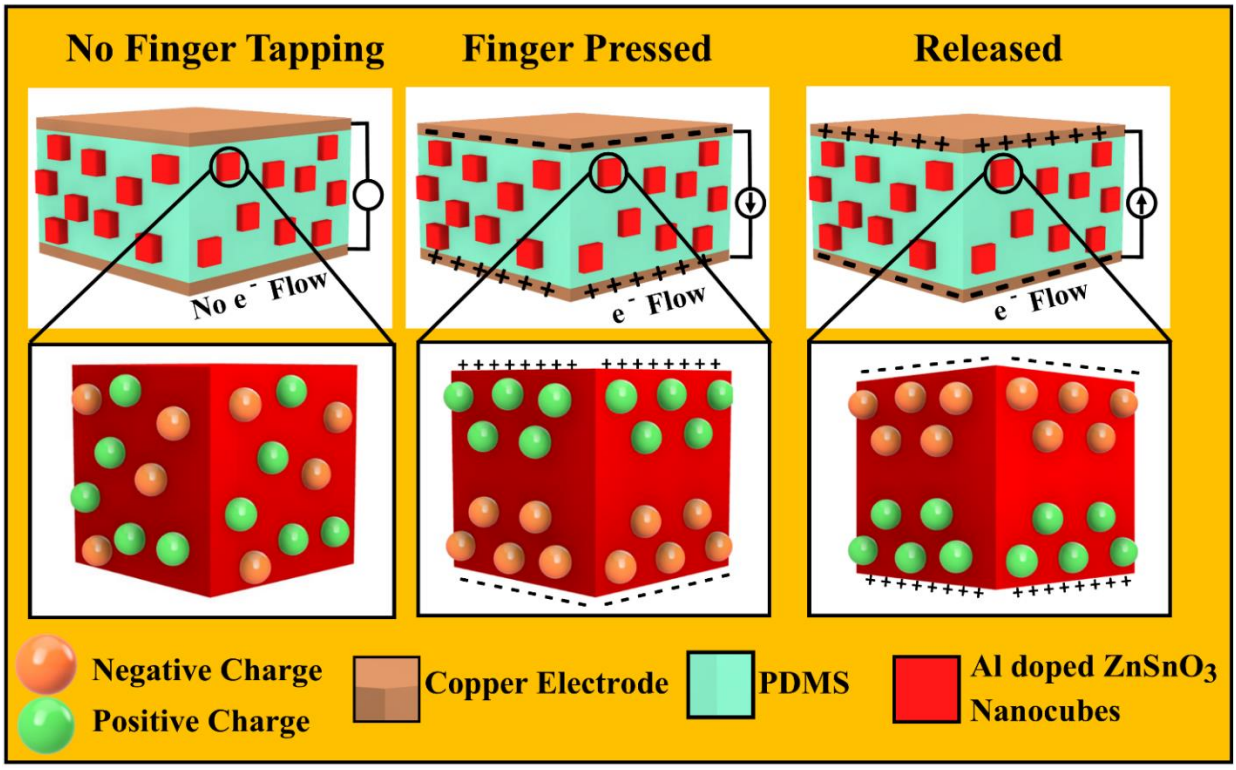

Figure 7: Schematic diagram of the working mechanism of the Al doped ZnSnO3 piezoelectric film.

This polarization can be attributed to $ZnSnO_3$'s non-centrosymmetric structure, which allows compression to shift the relative positions of cations and anions and create a dipole moment. Simultaneously, the resulting dipoles of each nanocubes unidirectionally align with each other, accumulating a significant potential difference between the top and bottom electrodes.

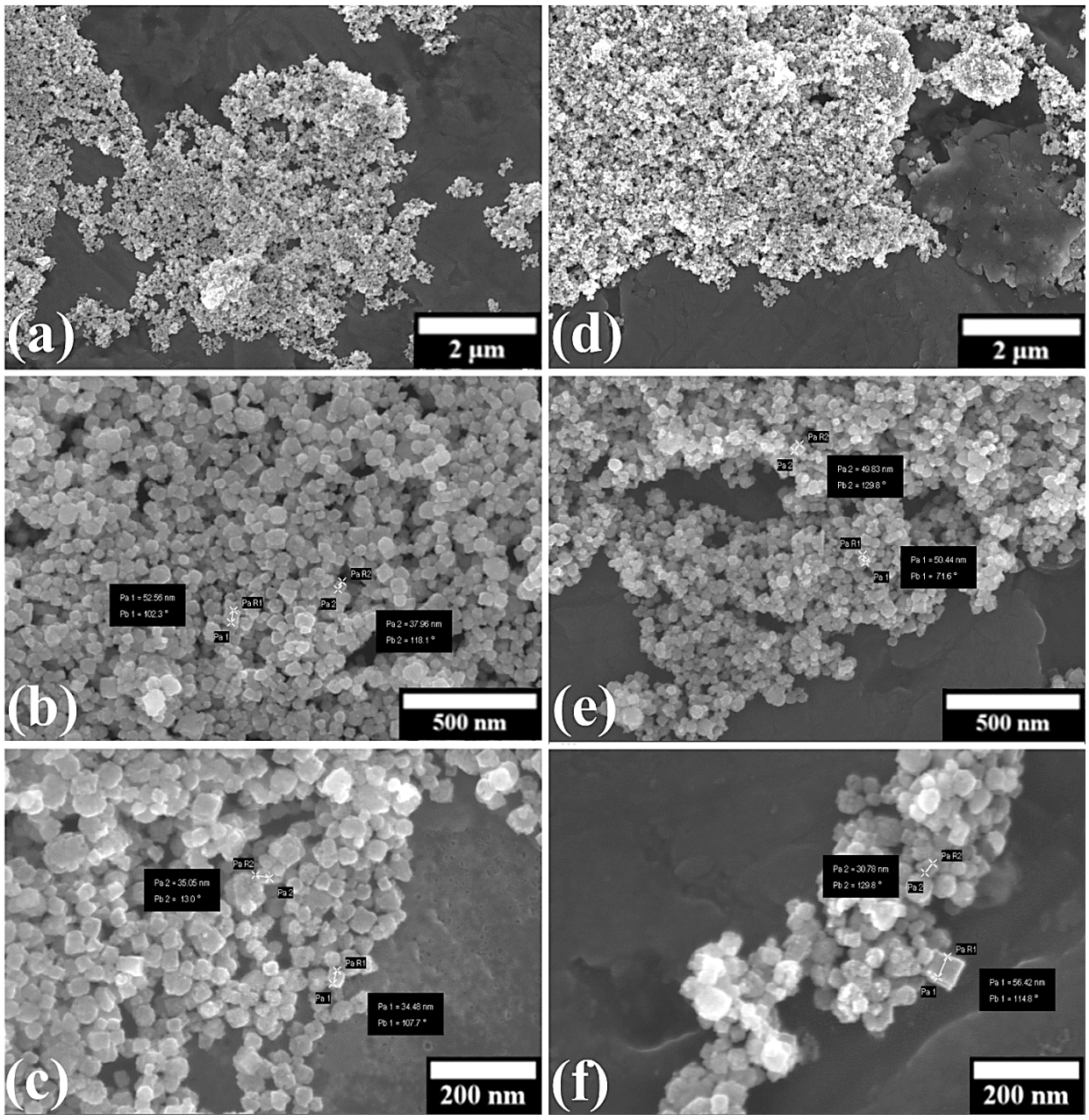

Figure 8: SEM images of undoped ZnSnO3 (a,b,c) and ZnSnO3 doped with 2% (w/w) of Al nanoparticles (d,e,f).

Thus, when the two electrodes are connected in a closed circuit, electrons flow from the negatively charged electrode to the positive one in an attempt to balance the charge. When the force is released, the ions within each nanocube briefly invert before return to their original distribution. Since electrons had once flowed to the positive electrode, that electrode now becomes negatively charged from the excess of electrons as the electric dipoles no longer align to sustain its original positive charge. There is a flow of electrons in the opposite direction compared to when the PENG was compressed. Thus, continuous compression and release creates alternating electrical current.

The morphology of synthesized samples was examined by SEM. Figure 8-(a), (b), and (c) show the SEM images of undoped $ZnSnO_3$, and (d), (e), and (f) are images for $ZnSnO_3$ doped with 2% (w/w) of Al. Formed particles are round-corner cubes, in the nanometer range. The size of the particles composed of undoped $ZnSnO_3$ is in the range of 35–50 nm, while for doped sample, the size ranges between 30–55 nm. After Al doping, size distribution of the nanomaterial increases. Which will clearly attribute to the electrical output properties of the doped ZnSnO3 piezoelectric film.

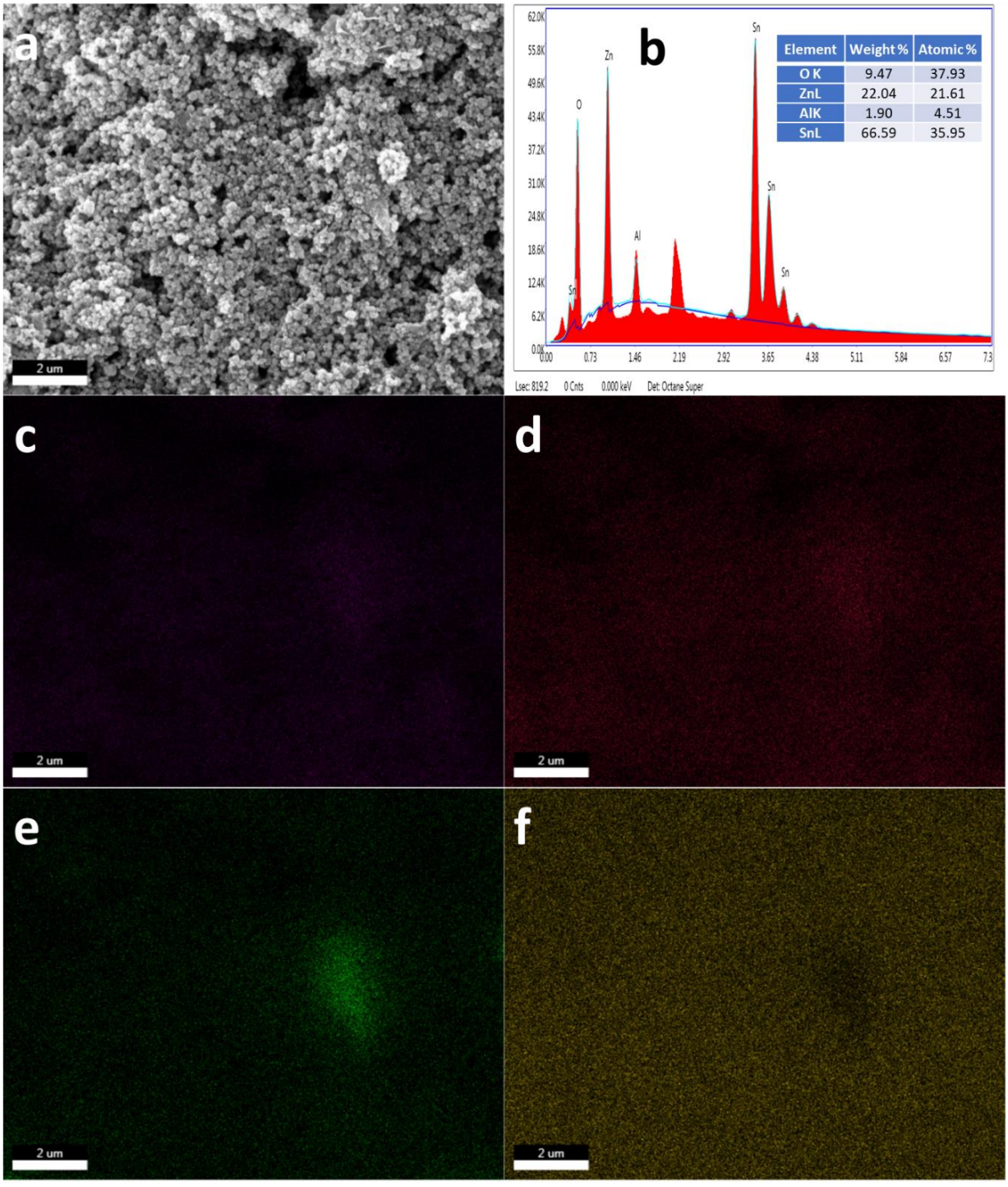

Figure 9: (a) SEM image, (b) EDX spectrum, (c) to (f) elemental mapping images of O, Zn, Al, and Sn, respectively.

In Figure 9 (a) the SEM image based on which EDX spectrum and elemental mapping images were obtained. The EDX spectrum (Figure 9-b) shows all the elements, i.e., O, Zn, Al, and Sn. Zn and Sn occupying L-shells were found at 1.01 and 3.44 eV, respectively. O and Al occupying K-shells were observed at 0.52 and 1.49 eV, respectively. The inset of Figure 9 (b) shows the table with the weight and atomic percentages of the elements present. The weight percent of Al is 1.90%. EDX spectrum and the inset table prove successful doping of Al in ZnSnO3. Figures 9(c) to 9(f) show the elemental mapping images which indicate the uniform distribution of these elements.

The XPS analysis is a useful tool for analyzing the material structure and surface chemical compositions. Figure 10 shows the survey scan XPS spectrum of $ZnSnO_3$ doped with 2% Al (w/w), and the one below has high-resolution spectra of the individual elements, i.e., Zn, Sn, O, and Al (Figure 10- (b) to (e), respectively). Binding energy (BE) in the survey scan spectrum has the range of 0–1300 eV and reveals all the elements. The peak with BE value 284.11 eV is assigned to C, and the source of C in the sample is CO_2 in the air. Al 2p peak has very low intensity, especially when comparing with Sn, Zn, and O peaks. The Sn 3d peak can be resolved into two peaks, i.e., Sn $3d_{5/2}$ at 486.97 eV and Sn $3d_{3/2}$ at 495.45 eV, which correspond to Sn in the sample. In the spectrum, we also observed Sn 4d, Sn $3d_{3/2}$, and Sn $3d_{1/2}$ signals at 28.15, 718.16, and 760.03 eV, respectively, which are due to different Sn orbitals in the sample. Note that in high-resolution spectra for Zn and Sn showed in the figure below, all peaks are deconvoluted into a single peak. A single component for each peak suggests that almost all Zn and Sn in the sample have the same oxidation states, i. e., Zn has oxidation state +2, and Sn has oxidation state +4, throughout the whole sample. The asymmetric O 1s can be split into two peaks. The peaks were observed at the BE values of 532.22 and 530.82 eV related to the oxygen

atoms in the form of Sn–O–Sn and Zn–O–Sn, respectively. Therefore, the XPS results apparently shows the uniformity of the sample.

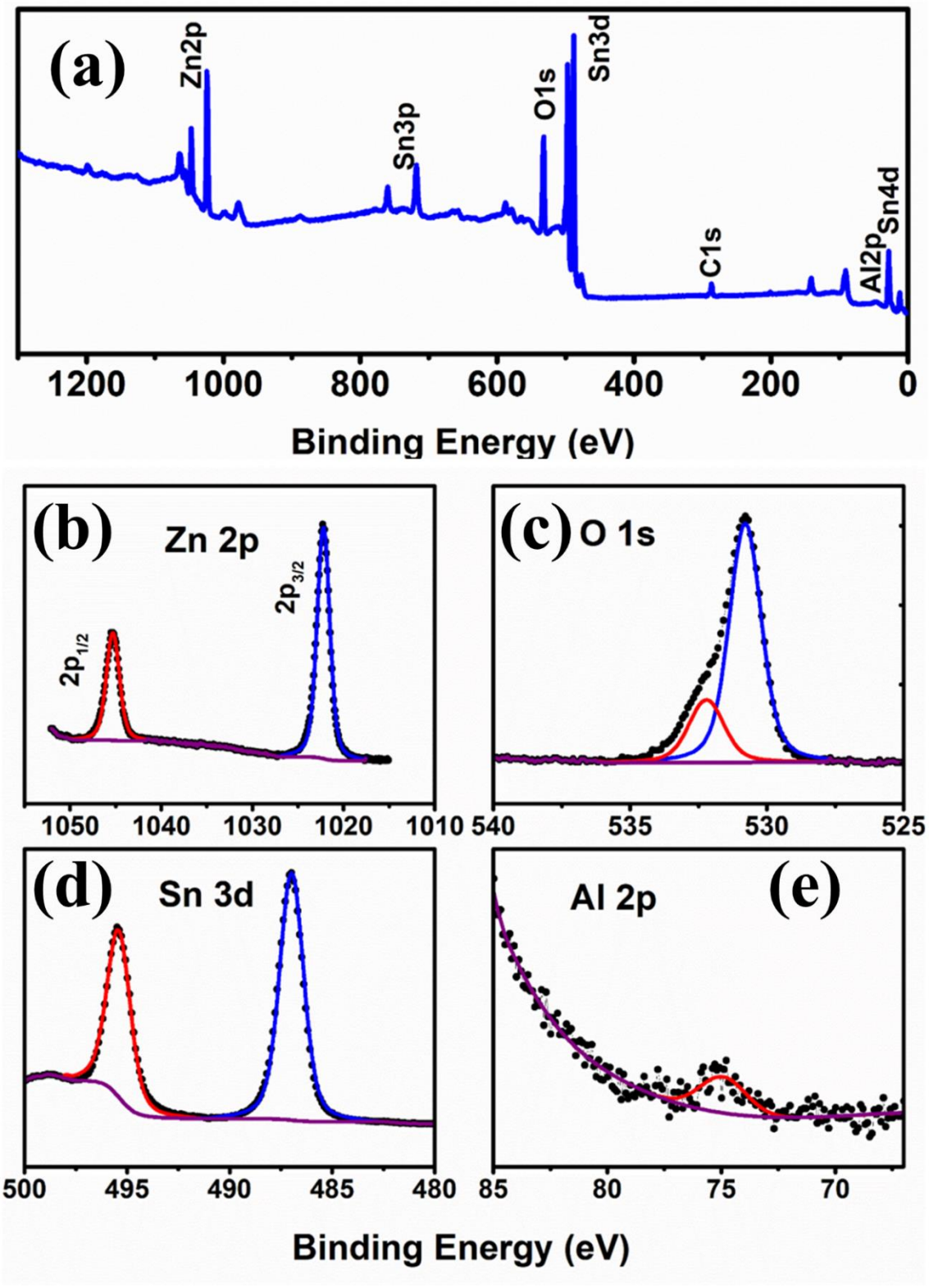

Figure 10: (a) Shows the survey scan XPS spectrum of ZnSnO3 doped with 2% Al (w/w), and the high-resolution spectra of the individual elements, i.e., (b) Zn, (c) O, (d) Sn, and (e) Al.

Figure 11 shows the XRD patterns of undoped $ZnSnO_3$. The sample shows XRD patterns with very similar peaks that can be successfully assigned to $ZnSnO_3 \cdot 4H_2O$ (ICDD PDF no. 00-028-1487). The peaks that appear at 2θ = 23.5°, 33.3°, 37.1°, 39.0°, 40.8°, 47.3°, 51.9°, 53.2°, 58.8°, and 62.7° match very well with the reference card. Also, the peak at 47.3° is present in both sample XRD and $ZnSnO_3 \cdot 4H_2O$ reference, while absent in peaks for cubic $ZnSn(OH)_6$ (ICDD PDF no. 00-033-1376). Thus, the XRD patterns of the synthesized alloy should mainly contain $ZnSnO_3 \cdot 4H_2O$.

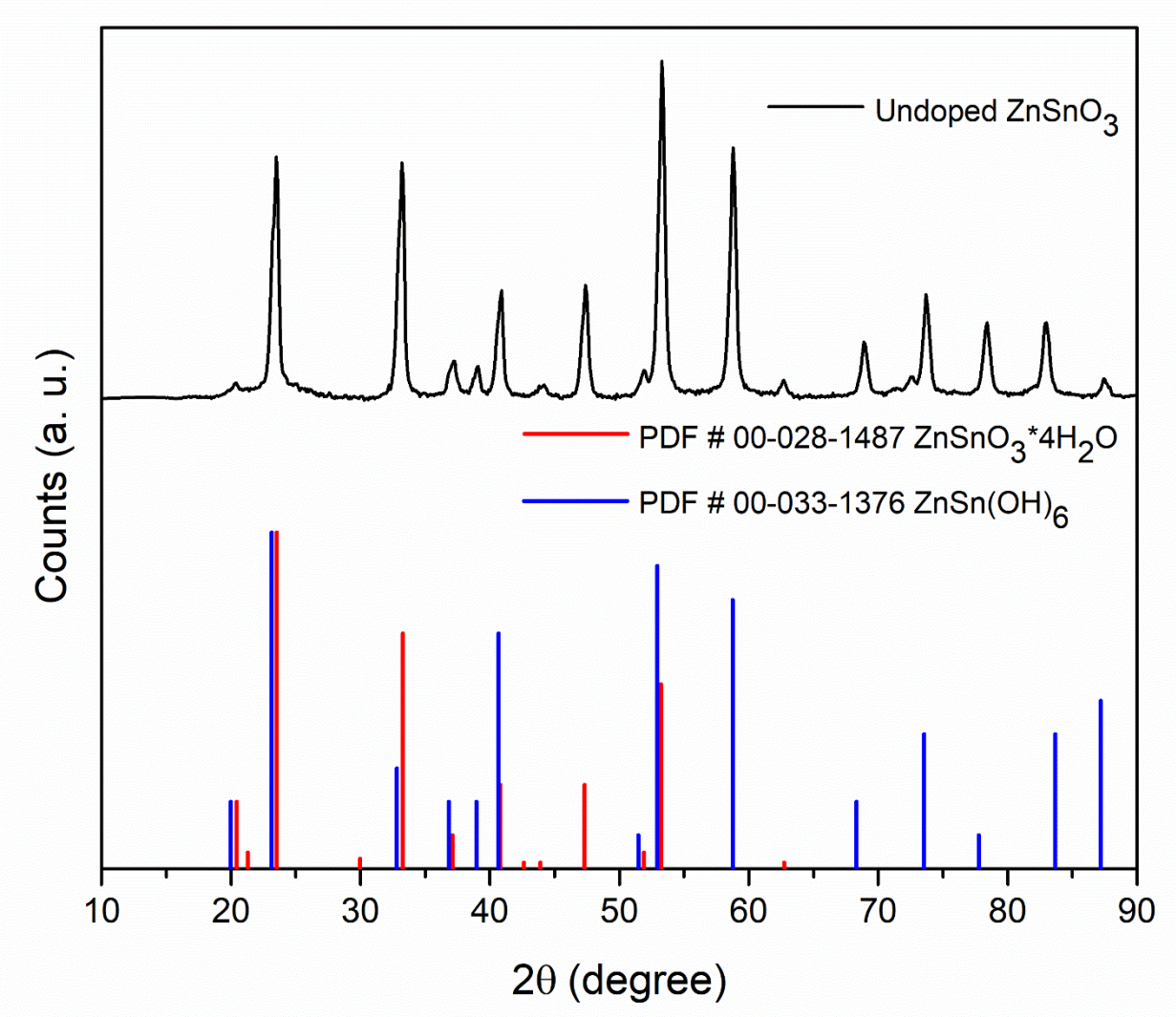

Figure 11: XRD patterns of undoped ZnSnO3 along with XRD peak positions for ZnSnO3·4H2O and ZnSn(OH)6.

The effects of Al dopant concentration of $ZnSnO_3$ on the piezoelectric output were systematically investigated by testing various PENGs with doped weight percentages ranging from 0 to 5%. The finger tapping frequency and approximate force were held constant to best isolate the effect of Al doping. The results for the time-dependent open circuit voltage (V_{OC}) can be seen in Figure 12 (a) at a finger tapping load frequency of 120 BPM. Similar data has been acquired for various finger tapping load frequencies, such as 60 BPM, 180 BPM, and 240 BPM. The results are enlisted in Figure 13- (a) to (c). With no aluminum doping (0 wt% Al), the Al doped $ZnSnO_3$ PENG achieved a positive V_{OC} of ~50V, which steadily increased to ~90V and ~110V at 1 wt% and 2 wt% of Al, respectively. Thus, Al doping of $ZnSnO_3$ can markedly improve the V_{OC} of the PENG, at least in smaller concentrations. Indeed, from 3 wt% and onwards, the output began decreasing at each interval of concentration, from ~70V to ~60V; 5 wt%, the voltage was ~40V, which was even lower than the pristine $ZnSnO_3$ nanogenerator. The addition of Al must be carefully measured as excessive amounts are detrimental to performance. Overall, the largest increase in voltage occurred in that initial 1 wt% addition of Al, but it eventually began tapering and decreasing when more dopant was added until the treatment became disadvantageous.

Figure 12 (b, c) shows that the short circuit current (I_{SC}) and power density followed this general trend as well. For the 2wt% Al-doped PENG, the short circuit current of ~13 μA. I_{sc} at various finger tapping frequencies (60 BPM, 180 BPM, 240 BPM) are also recorded and have been enlisted in the Figure 14- (a) to (c).

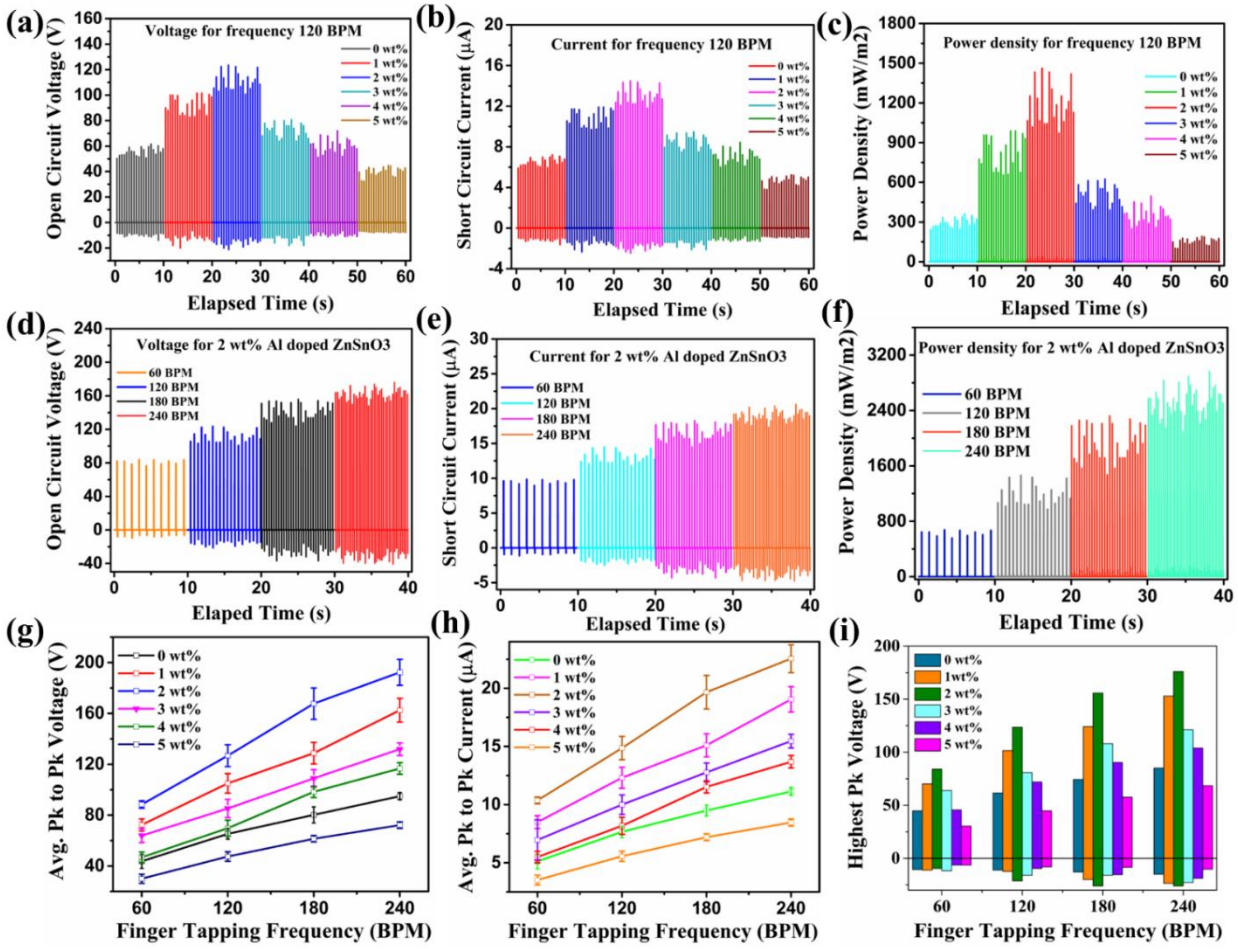

Figure 12: (a) The open circuit voltages, (b) short circuit currents, and (c) power density of PENGs with various concentrations of Al doping in ZnSnO3. (d) The open circuit voltages, (e) short circuit currents, and (f) power density for a PENG doped with 2 wt% a at various finger tapping frequencies. (g) The average peak to peak voltages, and (h) currents for all ranges of Al doping Concentration in ZnSnO3 at various finger tapping frequencies. (i) The Peak voltages for all ranges of Al doping Concentration in ZnSnO3 at various frequencies. (ZnSnO3 Piezoelectric film dimension 3.5cm×3.5 cm).

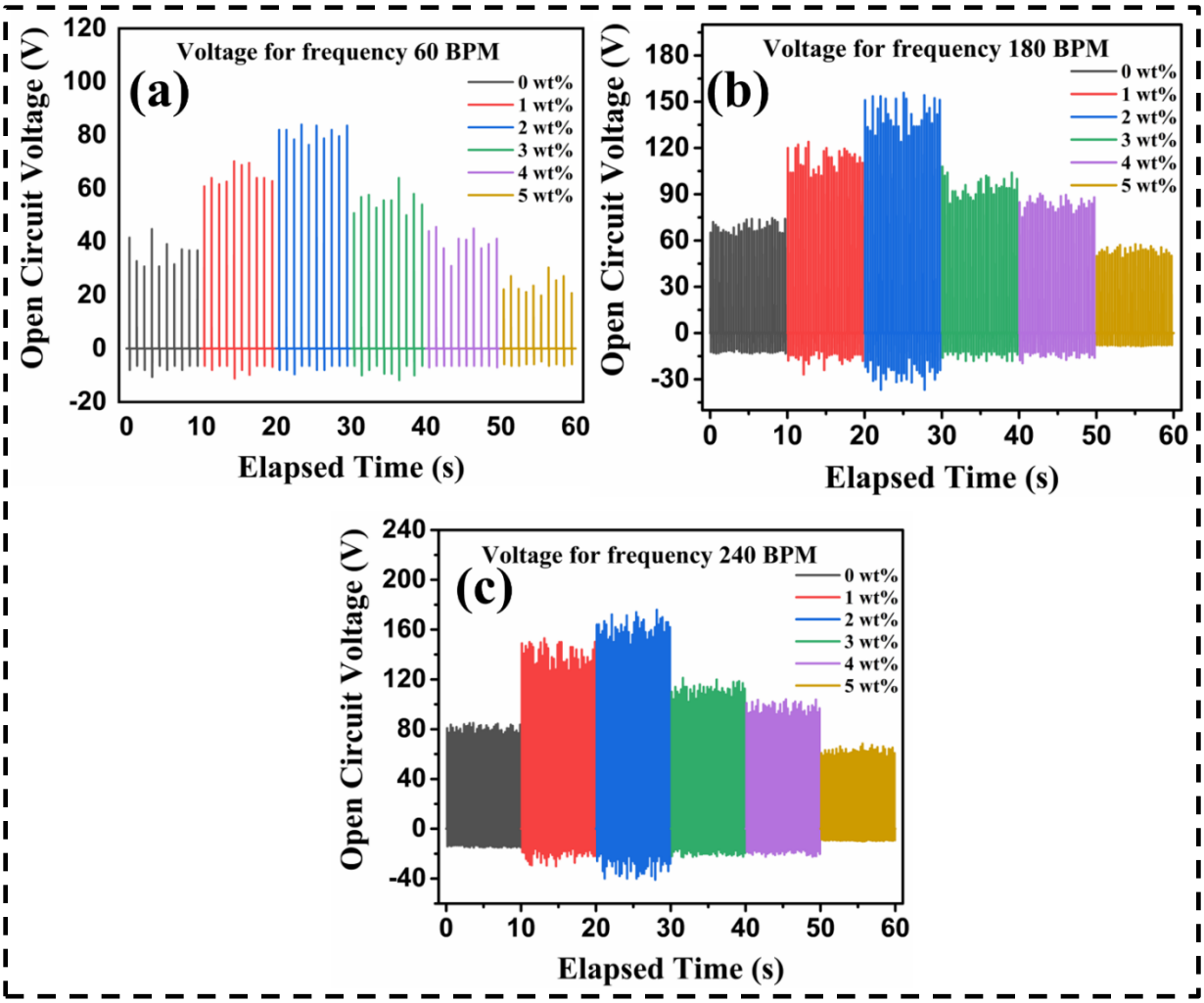

Figure 13: Open circuit Voltage at the finger tapping load frequency of (a) 60 BPM, (b) 180 BPM, and (c) 240 BPM

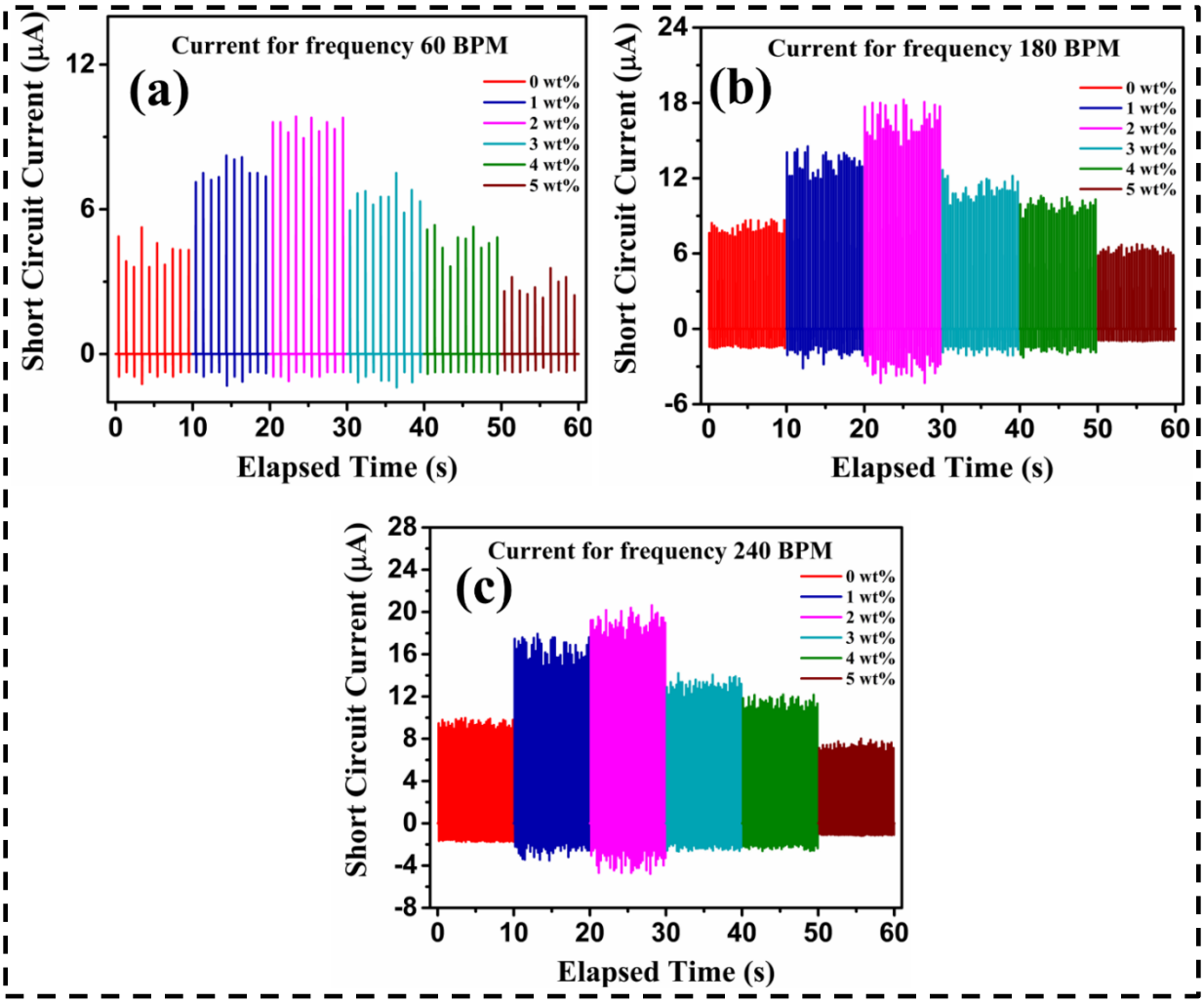

Figure 14: Short circuit Current at the finger tapping load frequency of (a) 60 BPM, (b) 180 BPM, and (c) 240 BPM

The differences of power density between concentrations were of greater magnitude than either measurement. The optimal concentration provided a power density of ~1200 mW/m^2, which was about four times greater than the undoped PENG at ~300 mW/m^2. This relationship is consistent with the previous result of roughly a two-fold increase for both voltage and current. The high power density of the PENG shows its feasibility as a miniature, portable power source.

This paper proposes one explanation for the decreasing output as the density increased beyond 2 wt%. Since aluminum itself does not have piezoelectric properties, the drawbacks of its increasing concentration (which decreases that of $ZnSnO_3$) eventually outweigh the enhancement it provides. Since the output peaked there, it can be reasonably concluded that 2 wt% of Al dopant is the optimal amount for electrical power generation.

Additionally, the output performance of 2 wt% Al doped $ZnSnO_3$ PENG was further evaluated for different finger-tapping frequencies. As seen in figure 12 (d), starting at a rate of 60 BPM, the PENG produced a positive open circuit voltage of ~80V which steadily increased to ~100V, ~130V, and ~150V with every additional 60 BPM. For this reason, comparing the effect of Al dopant concentration on output performance required that the frequency of mechanical disturbance be held constant, preventing it from skewing the results. Figure 12 (e, f) shows that I_{sc} and power density also increased approximately linearly with higher frequencies, starting with an output of ~10 μA at 60 BPM and reaching ~18 μA at 240BPM. The overall increase in output is consistent with previous literature and be attributed to a decrease in impedance caused by the higher tapping frequency, which leads to better impedance matching and power transfer [62]. The ability of the most optimally Al doped PENG to generate considerable electrical output at a variety of frequencies demonstrates its feasibility in applications involving the ambient environment, where the available mechanical disturbances in the ambient environment are likely to be unpredictable.

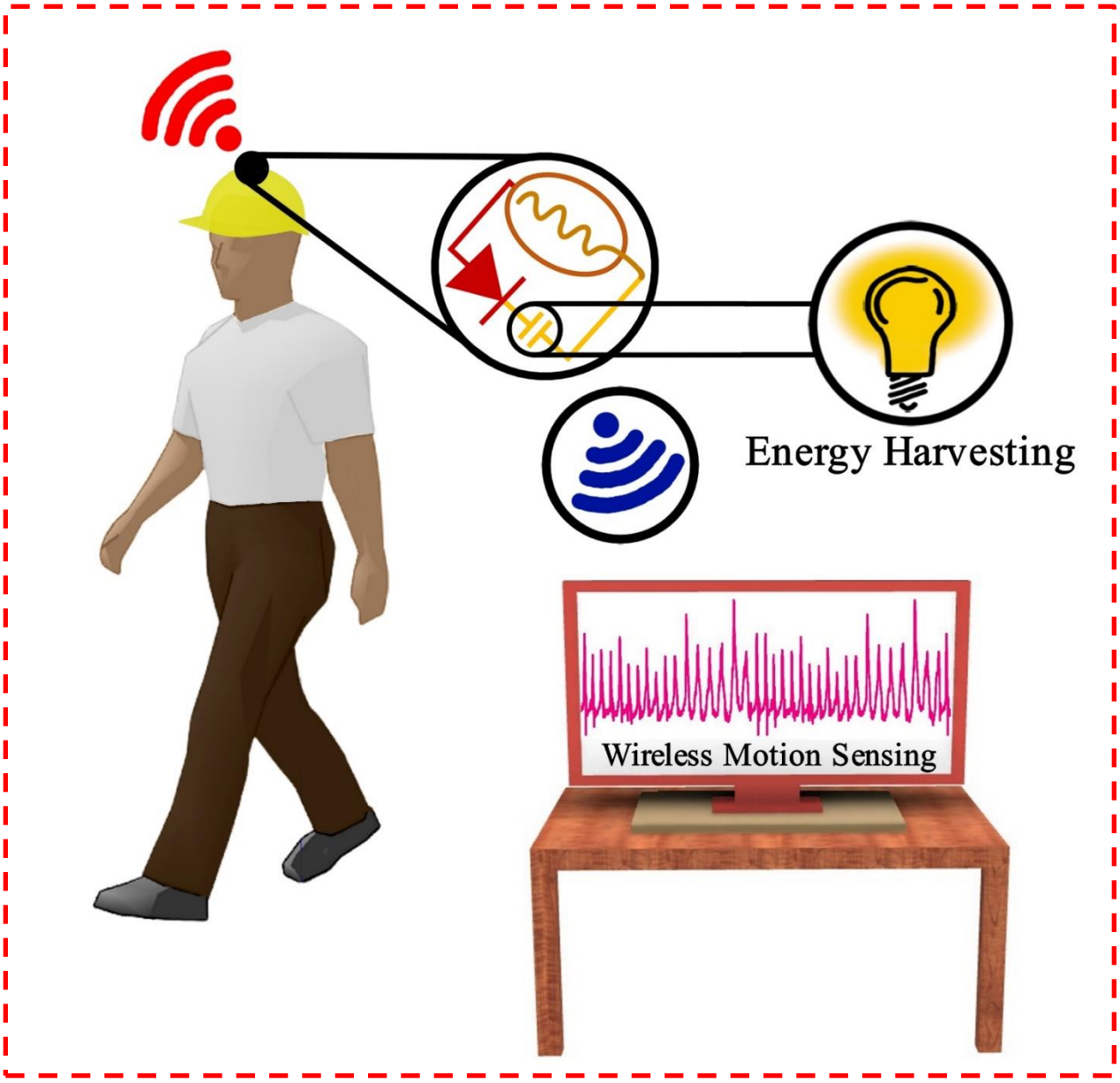

Figure 15: Schematic diagram of the application of the Al doped ZnSnO3 piezoelectric film, incorporated in a helmet to harvest energy and achieve wireless motion sensory application.

Each wt% of Al doped PENG responds similarly in terms of output when the frequency is increased. The impact of both the wt% of Al dopant and the frequency of finger tapping on peak to peak voltage ($V_{Pk\text{-}Pk}$) and current ($I_{Pk\text{-}Pk}$) is summarized in Figure 12 (g, h). The 2 wt% Al

doped PENG had the highest average V_{Pk-Pk} and I_{Pk-Pk}, which was approximately double that of the pristine PENG at nearly every frequency. The lowest performance was at 5 wt% Al doping. Additionally, from 60 to 240 BPM, a 4-fold increase, the output average $V_{Pk-Pk,}$ and I_{Pk-Pk} roughly doubled. Figure 12 (i) illustrates the highest peak voltages from each wt% Al doped PENG at every frequency, the absolute highest voltage recorded being 176 V.

The PENG's feasibility as a portable power source and energy harvester was also evaluated (Figure 15). To make the output from the PENG more useful for such a purpose, the alternating current was rectified to a direct current, which is more appropriate to power portable and wearable electronic devices. As seen in Figure 16 (a) and (b) the rectified voltage and current of the device declined compared to the AC voltage and current in Figure 12 (a) and (b) due to a dissipation of energy occurring as the current passes through the bridge rectifier diodes.

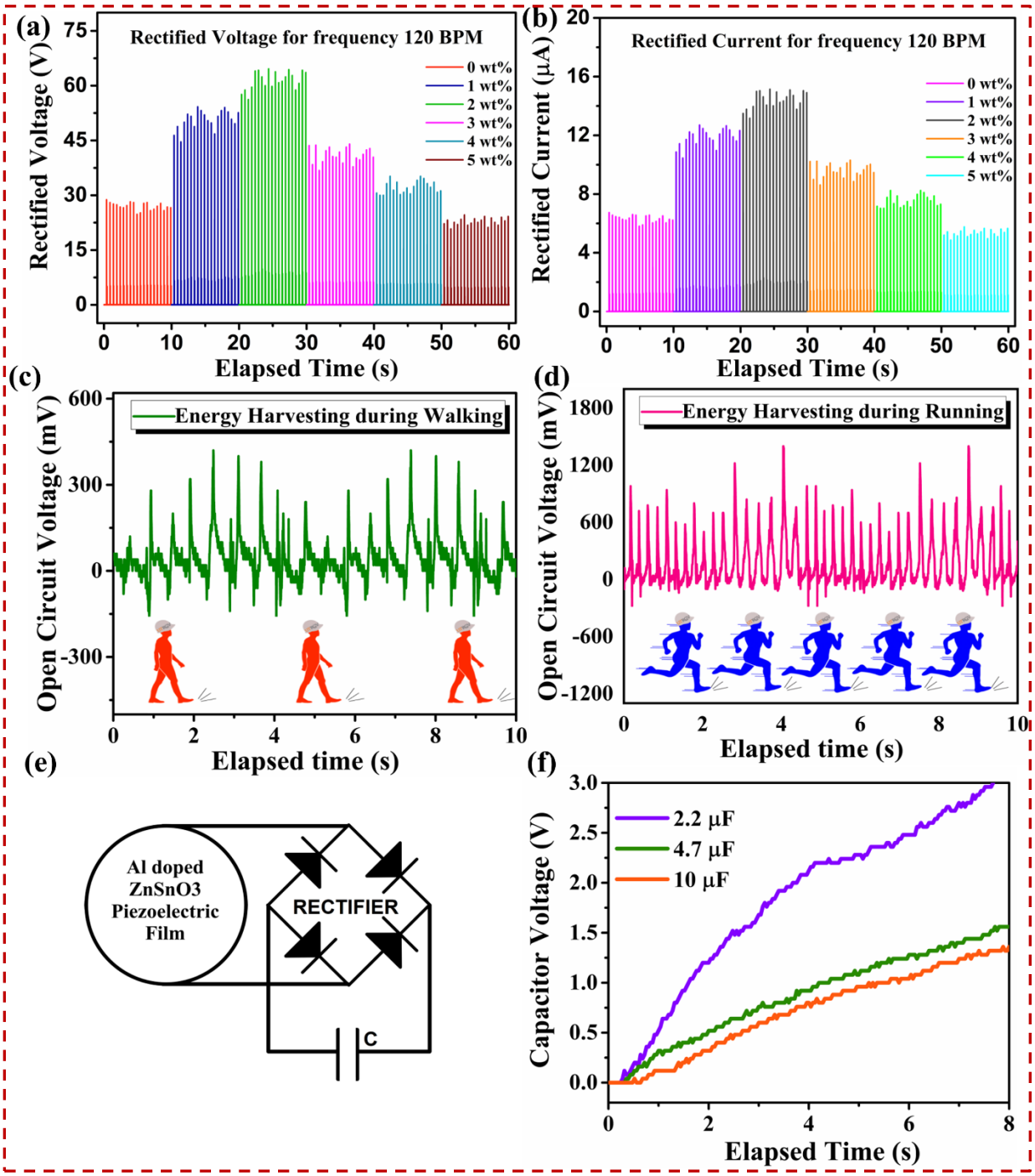

Figure 16: (a) Rectified voltage, and (b) current for all the doping concentrations at the finger tapping frequency of 120 BPM. (c) The open circuit voltages during walking, and (d) running with the smart helmet. (e) Circuit diagram of the Al doped ZnSnO3 PENG connected to a rectifier to

charge a capacitor. (f) The voltage levels of a 2.2 μF, 4.7 μF, and 10 μF capacitor in respect to the time for which the PENG charges them at a random finger tapping frequency.

The Al doped PENG was installed to the inside of a helmet to allow the device to seamlessly convert the energy from human motion, namely walking and running. The arrangement demonstrates one way in which the PENG can be used as an energy harvester. In Figure 16 (c), the output of the device reached up to 400 mV when walking, being compressed from the momentum of each step. The output in such minute compression during random walking and running clearly indicates the high size to response ratio of the device.

The real-time details of the helmet's energy harvesting feature have been recorded in a video file. In this case, the value of the PENG lies in its ability to steadily capture energy unobtrusively and over an extended period. In contrast, when the wearer of the helmet was running in Figure 16 (d), the peak voltage reaches ~1200 mV, as the compressions on the device increased in frequency. The increase in electrical output while running due to higher frequency compression and relaxation of the device into the helmet can be referred to the similar explanation as for the higher outputs obtained for finger tapping and has been already discussed in the prior sections.

Interestingly, the unique patterns of voltage peaks from Figure 16 (c, and d) also demonstrate that the PENG can be used as a self-powered motion sensor. Both the frequency of steps and the relative magnitude of the footstep force can be indicated. Since the output of a PENG, especially in the ambient environment as an energy harvester, can be inconsistent, a way to store the energy generated is important to their practical application. Figure 16 (e) shows one arrangement in which the PENG is connected to a bridge rectifier and capacitor. The capacitance-voltage graph, when charged by a PENG under finger-tapping, is illustrated in

Figure 16 (f). The device was capable of charging capacitors. Tested with 3 capacitors it showed to reach output capacitance voltage of 3V for 2.2 μF in only 8 seconds. At this same time capacitance voltage reaches ~1.5V and ~1.0V for the case of capacitors with a capacitance range of 4.7 μF and 10.0 μF respectively.

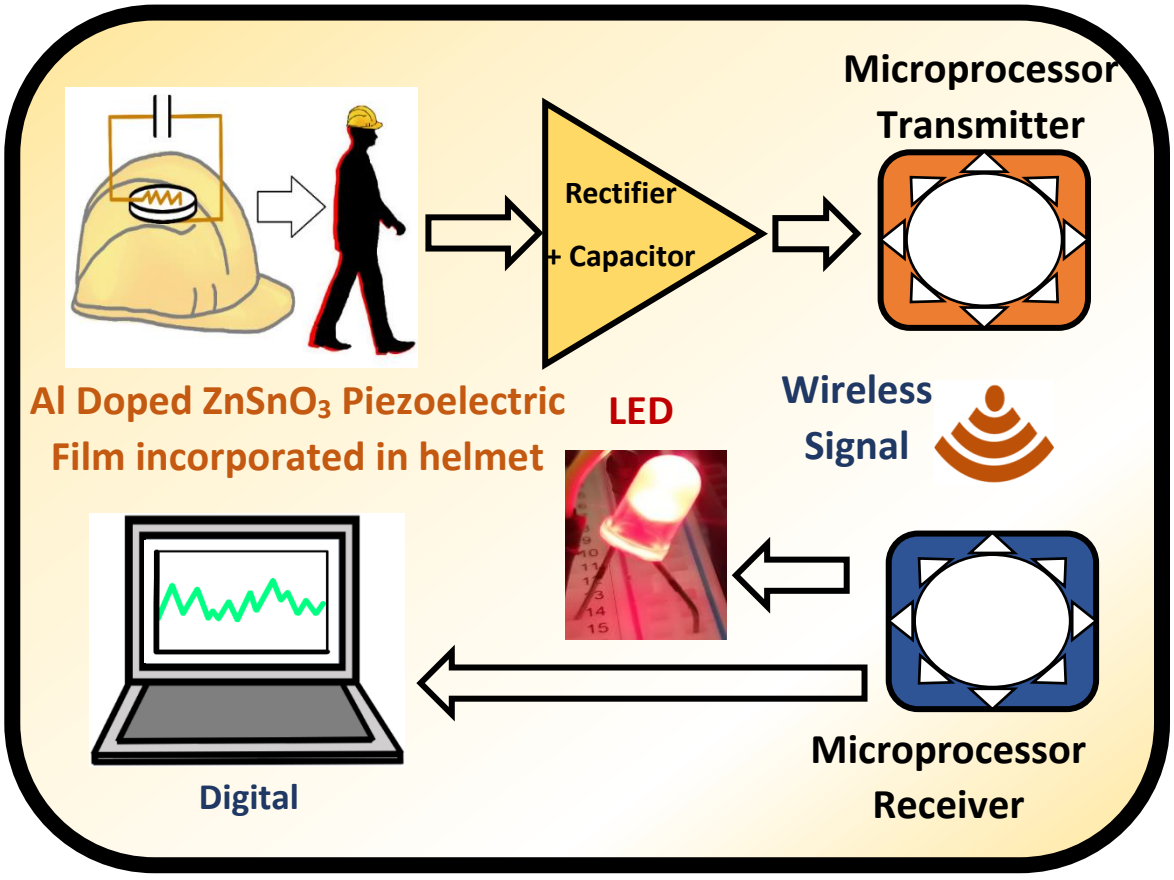

Figure 17: Schematic diagram for a motion sensing system using the Al doped PENG.

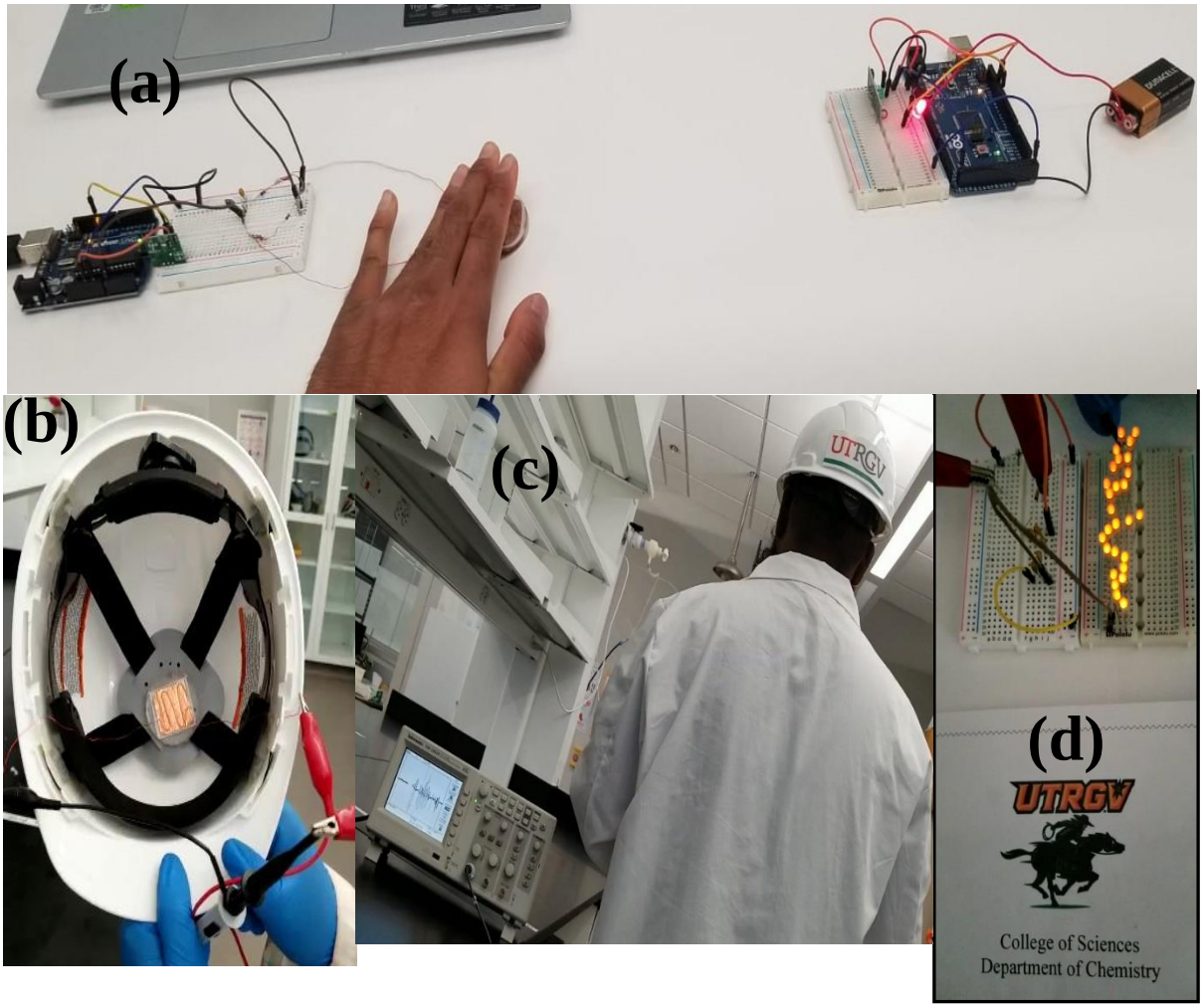

Figure 18: (a) An image of a microprocessor transmitter (on the left) attached to the cell and microprocessor receiver (on the right). (b) A helmet with an Al doped ZnSnO3 piezoelectric film incorporated, and (c) motion (Walking and Running) detection in terms of open circuit voltage with an oscilloscope using the helmet-PENG arrangement. (d) Random figure tapping of the Al doped ZnSnO3 piezoelectric film harvests energy to lit 28 LEDs.

In addition to its energy harvesting capacities, the Al doped ZnSnO3 nanogenerator can also be used in sensory applications, particularly for detecting the motion of any nature. This function is due to its ability to spontaneously respond to mechanical stress with an electrical output, and the lack of requirement for a battery or other external power source bestows the device's advantages over other sensors that are power-dependent.

For example, our PENG can continuously operate for longer and be made more compact. One such motion sensing system to detect human gait is illustrated in Figure 17. The PENG is attached to the top inside of a helmet, with its AC signal passed through a rectifier to convert it into a DC signal rectified. The PENG sensors placed parallel to the rectifier and capacitor, read the voltage and send it to a microprocessor (MP), which sends a wireless signal through a radio frequency (RF) transmitter when it reads the signal. After reaching the RF receiver paired with another MP, the wireless signal prompts that MP to turn on an LED, indicating that the PENG is generating voltage.

The information can be displayed in two ways: dichotomously (i.e., with the LED light, ‘on’ for motion and ‘off’ for motionless) or continuously (having the generated signal being displayed on a laptop).

Figure 18 (a) is a physical representation of the idea presented in Figure 17, where finger tapping on the PENG connected to a transmitter wirelessly turns on a LED connected to a receiver acting as a switch. Of course, as soon as there is no compression on the PENG, the LED turns off. Figure 18 (b) shows the PENG being attached to a helmet, and the unit was worn on the head and tested to detect walking. As shown in Figure 18 (c), the voltage generated by the PENG can indeed be recorded wirelessly. When the helmet and PENG device were worn, the electrical output of the PENG when walking was able to be displayed on Tektronix TDS 1001B oscilloscope. As a demonstration of the output capabilities of the PENG, it was able to light 28 LEDs with only finger tapping as seen in Figure 18 (d). This test demonstrates the sensitivity of the device, being able to generate large voltages with little input force required.

CHAPTER V

CONCLUSION

The development and usage of nanogenerators has been readily accepted and widely sought for due to their cost-effective structure and adept mechanisms. The initial fabrication of a PENG device began over a decade ago, and research has continued to invest efforts to further innovate it. Despite the continued research and the considerable output improvements, it has not yet achieved a sufficient generation of electricity to realize powering of portable devices. Moreover, the energy harvesting and sensory abilities it holds can be applied to in a diversity of areas, such as sensors. In this article, we have demonstrated an unprecedented, high-performance nanogenerator by incorporating aluminum-doped zinc stannate ($ZnSnO_3$) nanocubes (30nm-60nm) into PDMS.

The electrical output of the $ZnSnO_3$/PDMS-based film was ensured and further enhanced by doping zinc stannate with aluminum nanoparticles, and by adopting a low-temperature method, the product outcome resulted in a dependable synthesis of $ZnSnO_3$ nano-cubical structures. Moreover, $ZnSnO_3$ was doped with 1 wt% to 5 wt% of aluminum nanoparticles. Resultantly, we were able to report that 2 wt% of aluminum-doped $ZnSnO_3$ showed the highest electrical output in terms of open circuit voltages and short circuit current. The piezoelectric nanogenerator device attained an average, open-circuit voltage of 80 V to 175 V, with a frequency range of 60 BPM to 240 BPM. Zinc stannate ($ZnSnO_3$) is a multifunctional

semiconductor and proves to be promising in the field of energy harvesting. Moreover, the future utilization of piezoelectric nanogenerators and sustainable energy share a conjoined prospect of success.

REFERENCES

[1] Y. Feng, L. Zhang, Y. Zheng, D. Wang, F. Zhou, W. Liu, Leaves based triboelectric nanogenerator (TENG) and TENG tree for wind energy harvesting, Nano Energy 55 (2019) 260-268.

[2] N.S. Lewis, Toward cost-effective solar energy use, science 315(5813) (2007) 798-801.

[3] Z.L. Wang, Self-powered nanotech, Scientific American 298(1) (2008) 82-87.

[4] M. Bariya, H.Y.Y. Nyein, A. Javey, Wearable sweat sensors, Nature Electronics 1(3) (2018) 160-171.

[5] J. Chen, J. Yang, Z. Li, X. Fan, Y. Zi, Q. Jing, H. Guo, Z. Wen, K.C. Pradel, S. Niu, Networks of triboelectric nanogenerators for harvesting water wave energy: a potential approach toward blue energy, ACS nano 9(3) (2015) 3324-3331.

[6] B.D. Chen, W. Tang, C. He, C.R. Deng, L.J. Yang, L.P. Zhu, J. Chen, J.J. Shao, L. Liu, Z.L. Wang, Water wave energy harvesting and self-powered liquid-surface fluctuation sensing based on bionic-jellyfish triboelectric nanogenerator, Materials today 21(1) (2018) 88-97.

[7] J. Zhang, Z. Fang, C. Shu, J. Zhang, Q. Zhang, C. Li, A rotational piezoelectric energy harvester for efficient wind energy harvesting, Sensors and Actuators A: Physical 262 (2017) 123-129.

[8] J.-G. Sun, T.-N. Yang, C.-Y. Wang, L.-J. Chen, A flexible transparent one-structure tribo-piezo-pyroelectric hybrid energy generator based on bio-inspired silver nanowires network for biomechanical energy harvesting and physiological monitoring, Nano Energy 48 (2018) 383-390.

[9] M.J. Alam, S.M.A.Z. Shawon, M. Sultana, M.W. Rahman, M.M.R. Khan, Kinetic study of biodiesel production from soybean oil, 2014 POWER AND ENERGY SYSTEMS: TOWARDS SUSTAINABLE ENERGY, IEEE, 2014, pp. 1-5.

[10] A. Manbachi, R.S. Cobbold, Development and application of piezoelectric materials for ultrasound generation and detection, Ultrasound 19(4) (2011) 187-196.

[11] X.-X. Yu, H. Yin, H.-X. Li, H. Zhao, C. Li, M.-Q. Zhu, A novel high-performance self-powered UV-vis-NIR photodetector based on a CdS nanorod array/reduced

graphene oxide film heterojunction and its piezo-phototronic regulation, Journal of Materials Chemistry C 6(3) (2018) 630-636.

[12] X.-X. Yu, H. Yin, H.-X. Li, W. Zhang, H. Zhao, C. Li, M.-Q. Zhu, Piezo-phototronic effect modulated self-powered UV/visible/near-infrared photodetectors based on CdS: P3HT microwires, Nano Energy 34 (2017) 155-163.

[13] Z.L. Wang, Self-powered nanosensors and nanosystems, Wiley Online Library, 2012.

[14] G. Zhu, Z.-H. Lin, Q. Jing, P. Bai, C. Pan, Y. Yang, Y. Zhou, Z.L. Wang, Toward large-scale energy harvesting by a nanoparticle-enhanced triboelectric nanogenerator, Nano letters 13(2) (2013) 847-853.

[15] F. Yildiz, Potential Ambient Energy-Harvesting Sources and Techniques, Journal of technology Studies 35(1) (2009) 40-48.

[16] P. Niu, P. Chapman, R. Riemer, X. Zhang, Evaluation of motions and actuation methods for biomechanical energy harvesting, 2004 IEEE 35th annual power electronics specialists conference (IEEE Cat. No. 04CH37551), IEEE, 2004, pp. 2100-2106.

[17] M.M. Alam, A. Sultana, D. Mandal, Biomechanical and acoustic energy harvesting from TiO2 nanoparticle modulated PVDF nanofiber made high performance nanogenerator, ACS Applied Energy Materials 1(7) (2018) 3103-3112.

[18] A. Sultana, M.M. Alam, S.K. Ghosh, T.R. Middya, D. Mandal, Energy harvesting and self-powered microphone application on multifunctional inorganic-organic hybrid nanogenerator, Energy 166 (2019) 963-971.

[19] M.A. Johar, J.-H. Kang, M.A. Hassan, S.-W. Ryu, A scalable, flexible and transparent GaN based heterojunction piezoelectric nanogenerator for bending, air-flow and vibration energy harvesting, Applied energy 222 (2018) 781-789.

[20] S.M.A.Z. Shawon, A.X. Sun, V.S. Vega, B.D. Chowdhury, P. Tran, Z.D. Carballo, J.A. Tolentino, J. Li, M.S. Rafaqut, S. Danti, Piezo-Tribo Dual Effect Hybrid Nanogenerators for Health Monitoring, Nano Energy (2020) 105691.

[21] X. Cheng, X. Xue, Y. Ma, M. Han, W. Zhang, Z. Xu, H. Zhang, H. Zhang, Implantable and self-powered blood pressure monitoring based on a piezoelectric thinfilm: Simulated, in vitro and in vivo studies, Nano Energy 22 (2016) 453-460.

[22] R. Van Schaijk, R. Elfrink, J. Oudenhoven, V. Pop, Z. Wang, M. Renaud, A MEMS vibration energy harvester for automotive applications, Smart Sensors, Actuators, and MEMS VI, International Society for Optics and Photonics, 2013, p. 876305.

[23] D. Zhu, S.P. Beeby, M.J. Tudor, N.R. Harris, A credit card sized self powered smart sensor node, Sensors and Actuators A: Physical 169(2) (2011) 317-325.

[24] Z.L. Wang, J. Song, Piezoelectric nanogenerators based on zinc oxide nanowire arrays, Science 312(5771) (2006) 242-246.

[25] H. Liu, J. Zhong, C. Lee, S.-W. Lee, L. Lin, A comprehensive review on piezoelectric energy harvesting technology: Materials, mechanisms, and applications, Applied Physics Reviews 5(4) (2018) 041306.

[26] G.T. Hwang, V. Annapureddy, J.H. Han, D.J. Joe, C. Baek, D.Y. Park, D.H. Kim, J.H. Park, C.K. Jeong, K.I. Park, Self-powered wireless sensor node enabled by an aerosol-deposited PZT flexible energy harvester, Advanced Energy Materials 6(13) (2016) 1600237.

[27] R. Guo, Y. Guo, H. Duan, H. Li, H. Liu, Synthesis of orthorhombic perovskite-type ZnSnO3 single-crystal nanoplates and their application in energy harvesting, ACS applied materials & interfaces 9(9) (2017) 8271-8279.

[28] K.Y. Lee, D. Kim, J.H. Lee, T.Y. Kim, M.K. Gupta, S.W. Kim, Unidirectional high-power generation via stress-induced dipole alignment from ZnSnO3 nanocubes/polymer hybrid piezoelectric nanogenerator, Advanced Functional Materials 24(1) (2014) 37-43.

[29] M.M. Alam, S.K. Ghosh, A. Sultana, D. Mandal, Lead-free ZnSnO3/MWCNTs-based self-poled flexible hybrid nanogenerator for piezoelectric power generation, Nanotechnology 26(16) (2015) 165403.

[30] J. Xu, X. Jia, X. Lou, J. Shen, One-step hydrothermal synthesis and gas sensing property of ZnSnO3 microparticles, Solid-State Electronics 50(3) (2006) 504-507.

[31] A. Rovisco, A. dos Santos, T. Cramer, J. Martins, R. Branquinho, H. Águas, B. Fraboni, E. Fortunato, R. Martins, R. Igreja, Piezoelectricity Enhancement of Nanogenerators Based on PDMS and ZnSnO3 Nanowires through Microstructuration, ACS Applied Materials & Interfaces 12(16) (2020) 18421-18430.

[32] J.M. Wu, C. Xu, Y. Zhang, Y. Yang, Y. Zhou, Z.L. Wang, Flexible and Transparent Nanogenerators Based on a Composite of Lead-Free ZnSnO3 Triangular-Belts, Adv. Mater. (Weinheim, Ger.) 24(45) (2012) 6094-6099.

[33] J.M. Wu, C. Xu, Y. Zhang, Z.L. Wang, Lead-free nanogenerator made from single ZnSnO3 microbelt, ACS nano 6(5) (2012) 4335-4340.

[34] S. Paria, S. Ojha, S.K. Karan, S.K. Si, R. Bera, A.K. Das, A. Maitra, L. Halder, A. De, B.B. Khatua, Approach for enhancement in output performance of randomly oriented ZnSnO3 nanorod-based piezoelectric nanogenerator via p-n

heterojunction and surface passivation layer, ACS Appl. Electron. Mater. 2(8) (2020) 2565-2578.

[35] R. Guo, Y. Guo, H. Duan, H. Li, H. Liu, Synthesis of Orthorhombic Perovskite-Type ZnSnO3 Single-Crystal Nanoplates and Their Application in Energy Harvesting, ACS Appl. Mater. Interfaces 9(9) (2017) 8271-8279.

[36] G. Wang, Y. Xi, H. Xuan, R. Liu, X. Chen, L. Cheng, Hybrid nanogenerators based on triboelectrification of a dielectric composite made of lead-free ZnSnO3 nanocubes, Nano Energy 18 (2015) 28-36.

[37] M.M. Alam, S.K. Ghosh, A. Sultana, D. Mandal, Lead-free ZnSnO3/MWCNTs-based selfpoled flexible hybrid nanogenerator for piezoelectric power generation, Nanotechnology 26(16) (2015) 1-6.

[38] S. Paria, S.K. Karan, R. Bera, A.K. Das, A. Maitra, B.B. Khatua, A facile approach to develop a highly stretchable PVC/ZnSnO3 piezoelectric nanogenerator with high output power generation for powering portable electronic devices, Industrial & Engineering Chemistry Research 55(40) (2016) 10671-10680.

[39] Z. Wang, J. Liu, F. Wang, S. Chen, H. Luo, X. Yu, Size-controlled synthesis of ZnSnO3 cubic crystallites at low temperatures and their HCHO-sensing properties, The Journal of Physical Chemistry C 114(32) (2010) 13577-13582.

[40] S. Lee, J. Lee, W. Ko, S. Cha, J. Sohn, J. Kim, J. Park, Y. Park, J. Hong, Solution-processed Ag-doped ZnO nanowires grown on flexible polyester for nanogenerator applications, Nanoscale 5(20) (2013) 9609-9614.

[41] C. Liu, A. Yu, M. Peng, M. Song, W. Liu, Y. Zhang, J. Zhai, Improvement in the piezoelectric performance of a ZnO nanogenerator by a combination of chemical doping and interfacial modification, The Journal of Physical Chemistry C 120(13) (2016) 6971-6977.

[42] S. Lu, Q. Liao, J. Qi, S. Liu, Y. Liu, Q. Liang, G. Zhang, Y. Zhang, The enhanced performance of piezoelectric nanogenerator via suppressing screening effect with Au particles/ZnO nanoarrays Schottky junction, Nano Research 9(2) (2016) 372-379.

[43] S. Paria, S. Ojha, S.K. Karan, S.K. Si, R. Bera, A.K. Das, A. Maitra, L. Halder, A. De, B.B. Khatua, Approach for Enhancement in Output Performance of Randomly Oriented ZnSnO3 Nanorod-Based Piezoelectric Nanogenerator via p–n Heterojunction and Surface Passivation Layer, ACS Applied Electronic Materials 2(8) (2020) 2565-2578.

[44] A. Rovisco, A. Dos Santos, T. Cramer, J. Martins, R. Branquinho, H. Águas, B. Fraboni, E. Fortunato, R. Martins, R. Igreja, Piezoelectricity enhancement of nanogenerators based on PDMS and ZnSnO3 nanowires through

microstructuration, ACS applied materials & interfaces 12(16) (2020) 18421-18430.

[45] B. Dudem, L.K. Bharat, H. Patnam, A.R. Mule, J.S. Yu, Enhancing the output performance of hybrid nanogenerators based on Al-doped BaTiO 3 composite films: a self-powered utility system for portable electronics, Journal of Materials Chemistry A 6(33) (2018) 16101-16110.

[46] S. Danti, Boron nitride nanotubes as nanotransducers, Boron Nitride Nanotubes in Nanomedicine, Elsevier2016, pp. 123-138.

[47] S. Han, J. Kim, S.M. Won, Y. Ma, D. Kang, Z. Xie, K.-T. Lee, H.U. Chung, A. Banks, S. Min, Battery-free, wireless sensors for full-body pressure and temperature mapping, Science translational medicine 10(435) (2018) eaan4950.

[48] M. Lee, C.Y. Chen, S. Wang, S.N. Cha, Y.J. Park, J.M. Kim, L.J. Chou, Z.L. Wang, A hybrid piezoelectric structure for wearable nanogenerators, Advanced Materials 24(13) (2012) 1759-1764.

[49] C. Sun, Q. Shi, D. Hasan, M.S. Yazici, M. Zhu, Y. Ma, B. Dong, Y. Liu, C. Lee, Self-powered multifunctional monitoring system using hybrid integrated triboelectric nanogenerators and piezoelectric microsensors, Nano Energy 58 (2019) 612-623.

[50] S.K. Ghosh, D. Mandal, Efficient natural piezoelectric nanogenerator: electricity generation from fish swim bladder, Nano Energy 28 (2016) 356-365.

[51] S. Maiti, S.K. Karan, J.K. Kim, B.B. Khatua, Nature Driven Bio-Piezoelectric/Triboelectric Nanogenerator as Next-Generation Green Energy Harvester for Smart and Pollution Free Society, Advanced Energy Materials 9(9) (2019) 1803027.

[52] S. Maiti, S.K. Karan, J. Lee, A.K. Mishra, B.B. Khatua, J.K. Kim, Bio-waste onion skin as an innovative nature-driven piezoelectric material with high energy conversion efficiency, Nano Energy 42 (2017) 282-293.

[53] S.K. Ghosh, D. Mandal, Bio-assembled, piezoelectric prawn shell made self-powered wearable sensor for non-invasive physiological signal monitoring, Applied Physics Letters 110(12) (2017) 123701.

[54] Y. Fu, H. He, T. Zhao, Y. Dai, W. Han, J. Ma, L. Xing, Y. Zhang, X. Xue, A self-powered breath analyzer based on PANI/PVDF piezo-gas-sensing arrays for potential diagnostics application, Nano-micro letters 10(4) (2018) 76.

[55] W. Han, H. He, L. Zhang, C. Dong, H. Zeng, Y. Dai, L. Xing, Y. Zhang, X. Xue, A self-powered wearable noninvasive electronic-skin for perspiration analysis based on piezo-biosensing unit matrix of enzyme/ZnO nanoarrays, ACS Applied Materials & Interfaces 9(35) (2017) 29526-29537.

[56] X. Xue, Y. Fu, Q. Wang, L. Xing, Y. Zhang, Outputting olfactory bionic electric impulse by PANI/PTFE/PANI sandwich nanostructures and their application as flexible, smelling electronic skin, Advanced Functional Materials 26(18) (2016) 3128-3138.

[57] E. Aksel, J.L. Jones, Advances in lead-free piezoelectric materials for sensors and actuators, Sensors 10(3) (2010) 1935-1954.

[58] B. Azimi, M. Milazzo, A. Lazzeri, S. Berrettini, M.J. Uddin, Z. Qin, M.J. Buehler, S. Danti, Electrospinning piezoelectric fibers for biocompatible devices, Advanced Healthcare Materials 9(1) (2020) 1901287.

[59] G.T. Hwang, M. Byun, C.K. Jeong, K.J. Lee, Flexible piezoelectric thin-film energy harvesters and nanosensors for biomedical applications, Advanced healthcare materials 4(5) (2015) 646-658.

[60] L. Cheng, M. Yuan, L. Gu, Z. Wang, Y. Qin, T. Jing, Z.L. Wang, Wireless, power-free and implantable nanosystem for resistance-based biodetection, Nano Energy 15 (2015) 598-606.

[61] D. Xu, W. Li, L. Wang, W. Wang, W. Cao, W. Fei, Large piezoelectric properties induced by doping ionic pairs in BaTiO3 ceramics, Acta materialia 79 (2014) 84-92.

[62] C. Chang, V.H. Tran, J. Wang, Y.-K. Fuh, L. Lin, Direct-write piezoelectric polymeric nanogenerator with high energy conversion efficiency, Nano letters 10(2) (2010) 726-731.

BIOGRAPHICAL SKETCH

Sk Md Ali Zaker Shawon received his B.Sc. in Chemical Engineering from Jashore University of Science and Technology, Bangladesh in 2013. Then he joined as a "Process Engineer" in one of the biggest petrochemical company in Bangladesh. He started his Master's program in the department of Chemistry at the University of Texas Rio Grande Valley in 2019. Here he joined Photonics and Energy Research Laboratory as a Graduate Research Assistant. He also worked as a Teaching Assistant at the department of Chemistry. He was awarded a Master of Science in Chemistry from the University of Texas Rio Grande Valley in May of 2021. Currently, his research interests include application of nanostructured functional interfaces in hybrid nanogenerators, development of antimicrobial and antiviral textile fibers, dye sensitized solar cells, renewable energy, and electromechanical sensors. He can be reached at- azshawon@gmail.com.